HIGH-THROUGHPUT SELECTION OF MINERALIZING PEPTIDES

A Thesis Submitted to
the Graduate School of
İzmir Institute of Technology
in Partial Fulfillment of the Requirements for the Degree of

MASTER OF SCIENCE

in Materials Science & Engineering

by
Gizem ÇULHA

July 2024
İZMİR

We approve the thesis of **Gizem ÇULHA**

Examining Committee Members:

_____

Assoc. Prof. Fatih Toptan

Department of Materials Science and Engineering, Izmir Institute of Technology

_____

Asst. Prof. Deniz Tanıl YÜCESOY

Department of Bioengineering, Izmir Institute of Technology

_____

Prof. Dr. Yaşar AKDOĞAN

Department of Materials Science and Engineering, Izmir Institute of Technology

_____

Assoc. Prof. Ceyda Öksel KARAKUŞ

Department of Bioengineering, Izmir Institute of Technology

_____

Assoc. Prof. Hande KEMALOĞLU

Department of Restorative Dental Treatment, Ege University

2 July 2024

_____	_____
Assoc. Prof. Fatih TOPTAN	**Asst. Prof. Deniz Tanıl YÜCESOY**
Supervisor, Department of Materials Science and Engineering	Co-Supervisor, Department of Bioengineering
İzmir Institute of Technology	İzmir Institute of Technology
_____	_____
Prof. Dr. Yaşar AKDOĞAN	**Prof. Dr. Mehtap EANES**
Head of the Department of Materials Science and Engineering	Dean of the Graduate School of Engineering and Sciences

ACKNOWLEDGMENTS

First of all, I’m grateful to my advisor Assoc. Prof. Fatih Toptan for his support.

I would like to express my gratitude to my co-supervisor Dr. Deniz Tanıl Yücesoy for supporting, guiding and encouraging me during my research.

I would like to thank BAP (2021IYTE-1-0114 and 2022IYTE-2-0050) for their financial support during my master's studies.

I would like to thank TUBİTAK (2210-C) for their financial support for my research.

I extend my appreciation to all Yucesoy Lab members for their valuable supports. I specially thank to my colleague İlker Kan and Alp Deniz Öğüt for their motivation and endless support from the beginning.

Finally, I’m deeply grateful to my family for their constant trust and support throughout my life.

ABSTRACT

HIGH-THROUGHPUT SELECTION OF MINERALIZING PEPTIDES

Over 3.4 billion years of protein evolution, Mother Nature has refined molecular pathways that regulate and control biomineral formation. The exquisite hierarchical structures and multifunctional properties of biological hard tissues have long been inspired material scientists and engineers. These natural composites synthesized by proteins facilitate the nucleation and growth of inorganic solids, thereby directing mineral formation within organisms. Although biomineralization being essential for life, its dysregulation may lead to significant health issues. Understanding this mechanism is therefore crucial for developing treatments for diseases associated with abnormal mineral deposition. Inspired by biology at the nanoscale, the aim of this thesis was to identify short catalytic peptides that can govern hydroxyapatite (HAp) mineralization similar to natural proteins by deep directed evolution approach. Our results demonstrated the identification of several peptides with unique sequences. Structural characterization conducted through XRD and FTIR analyses confirmed the formation of hydroxyapatite in the presence of these peptides. Kinetic measurements further revealed that these peptides catalyze calcium phosphate mineralization 15 times faster under physiological conditions. The rapid mineralization kinetics exhibited by these peptides in an aqueous media supplemented with calcium and phosphate suggest a strong potential for restoring demineralized tissues and treating diseases related to pathological biomineralization. Furthermore, these peptide sequences could serve as foundational elements in the development of clinical products including dental gels and toothpaste formulations, as well as in treatments for bone regeneration and other medical applications where controlled mineralization is crucial.

ÖZET

MİNERALLEŞTİRİCİ PEPTİTLERİN YÜKSEK VERİMLİ SEÇİMİ

3,4 milyar yılı aşkın protein evrimi boyunca Doğa Ana, biyomineral oluşumunu düzenleyen ve kontrol eden moleküler yollar geliştirmiştir. Biyolojik sert dokuların mükemmel hiyerarşik yapıları ve çok işlevli özellikleri uzun süredir malzeme bilimcilerine ve mühendislerine ilham kaynağı olmuştur. Proteinler tarafından sentezlenen bu doğal kompozitler, inorganik katıların çekirdeklenmesini ve büyümesini kolaylaştırır ve böylece organizmalarda mineral oluşumunu yönlendirir. Biyomineralizasyon yaşam için gerekli olmasına rağmen; düzensizliği önemli sağlık sorunlarına yol açabilir. Bu nedenle, bu mekanizmayı anlamak anormal mineral birikimiyle ilişkili hastalıklara yönelik tedavilerin geliştirilmesi açısından çok önemlidir. Nano ölçekte biyolojiden ilham alan bu tezin amacı, derin yönelimli evrim yaklaşımıyla doğal proteinlere benzer şekilde hidroksiapatit (HAp) mineralizasyonunu yönetebilen kısa katalitik peptitleri tanımlamaktır. Sonuçlarımız, benzersiz dizilere sahip peptitlerin tanımlandığını gösterdi. XRD ve FTIR analizleri yoluyla yapılan yapısal karakterizasyon, bu peptitlerin varlığında hidroksiapatit oluşumunu doğruladı. Bununla birlikte, kinetik ölçümler bu peptitlerin fizyolojik koşullar altında kalsiyum fosfat mineralizasyonunu on beş kat daha hızlı katalize ettiğini ortaya çıkardı. Bu peptitlerin, kalsiyum ve fosfat ile desteklenmiş sulu ortamda sergilediği hızlı mineralizasyon kinetiği, demineralize olmuş dokuların onarılması ve patolojik biyomineralizasyon ile ilişkili hastalıkların tedavisi için güçlü bir potansiyele işaret etmektedir. Aynı zamanda, bu peptit dizileri, diş jelleri ve diş macunu formülasyonları dahil olmak üzere klinik ürünlerin geliştirilmesinde, kemik rejenerasyonu tedavilerinde ve kontrollü mineralizasyonun önemli olduğu diğer tıbbi uygulamalarda temel unsurlar olarak hizmet edebilir.

TABLE OF CONTENTS

LIST OF FIGURES

LIST OF TABLES

Table **Page**

ABBREVIATIONS

ACP	Amorphous Calcium Phosphate
ADP5	Amelogenin Derived Peptide 5
BP1-M1	Biopanning Round I- Mineralizing Peptide
BP1-M2	Biopanning Round I- Purified Mineralizing Peptide
BP1-S1	Biopanning Round I- Supernatant 1
BP2-M1	Biopanning Round II- Mineralizing Peptide
BP2-M2	Biopanning Round II- Purified Mineralizing Peptide
BP2-S1	Biopanning Round II- Supernatant 1
BP2-S2	Biopanning Round II- Supernatant 2 (/%0.01 detergent)
BP2-S3	Biopanning Round II- Supernatant 3 (/%0.01 detergent)
BP3-M1	Biopanning Round III- Mineralizing Peptide
BP3-M2	Biopanning Round III- Purified Mineralizing Peptide
BP3-S1	Biopanning Round III- Supernatant 1
BP3-S2	Biopanning Round III- Supernatant 2 (/%0.01 detergent)
BP3-S3	Biopanning Round III- Supernatant 3 (/%0.02 detergent)
BP4-M1	Biopanning Round IV- Mineralizing Peptide
BP4-M2	Biopanning Round IV- Purified Mineralizing Peptide
BP4-S1	Biopanning Round IV- Supernatant 1
BP4-S2	Biopanning Round IV- Supernatant 2 (/%0.01 detergent)
BP4-S3	Biopanning Round IV- Supernatant 3 (/%0.05 detergent)
Buffer EB	Elution Buffer
Buffer MP	M13 Precipitation Buffer
Buffer PB	M13 Lysis Buffer
Buffer PE	Wash buffer for Removal of Excess Salt
Ca/P	Calcium Phosphate
CNT	Classical Nucleation Theory
CPA	Crystallization by Particle Attachment
DCP	Dicalcium Phosphate
ER2738	*E. coli* strain
FTIR	Fourier Transform Infrared Spectroscopy

HABP1	Hydroxyapatite Binding Peptide I
HABP2	Hydroxyapatite Binding Peptide II
HABPs	Hydroxyapatite Binding Peptides
HAp	Hydroxyapatite
IPTG	Isopropyl-β-D-Thiogalactopyranosid
M13KE	Cloning Vector of 12-mer Phage Library
M13mp19	Cloning Vector
MCP	Monocalcium Phosphate
MP	Mineralizing Peptide
OCP	Octacalcium Phosphate
PEG	Poly-Ethylene Glycol
PILP	Polymer Induced Liquid Precursor
RM180	180 Aminoacid Amelogenin Protein
SEM	Scanning Electron Microscope
ssDNA	Single-Stranded DNA
TBS	Tris-Buffered Saline
TCP	Tricalcium Phosphate
XGAL	5-Bromo-4-Chloro-3-Indolyl-β-D-Galactopyranoside
XRD	X-Ray Diffraction
α-TCP	α-Tricalcium Phosphate
β-TCP	β-Tricalcium Phosphate

CHAPTER 1

INTRODUCTION

1.1. Biomineralization

Minerals are substances that are naturally formed through geological processes on Earth and serve as the building blocks of rocks and play a crucial role in various geological processes include crystallization, solidification or participation in chemical reactions (Figure 1.1.) (Kanazawa and Kamitani 2006). In order to be classifed as a mineral, a substance required to be naturally occurred, inorganic, solid at room temperature; have an ordered internal structure and a definite chemical composition. 99% of these minerals are composed of eight elements: oxygen, aliminium, calcium, potassium, silicon, iron, sodum and magnesium (Read 1970; Hänsch and Mendel 2009). Mother Nature has also refined molecular pathways that regulate the formation of the toughest materials ranging from mollusks shells to formation of eggshells in birds (calcium carbonate); bone to the teeth (calcium phosphate) (Table 1.1). The underlining process that results in the formation of these materials is termed as biomineralization. Biomineralization is a natural process wherein ions accumulate in formations along with organic protein molecules and facilitate nucleation and growth of inorganic solids, thereby directing mineral formation within organisms (Sharma et al. 2021). This process that enable proteins to produce minerals involves three essential steps:

Figure 1.1. Minerals.

Table 1.1. Major Categories of Biominerals;

Mineral	**Formula**	**Function**
Calcium Carbonate (Calcite, Aragonite, Vaterite)	$CaCO_3$	Construct Exoskeleton (Mollusk, Corals and Algae)
Calcium Phosphate (Hydroxyapatite)	$Ca_3(PO_4)_2$	Endoskeleton, Teeth, Calcium and Phosphate Storage
Calcium Oxalate	CaC_2O_4	Calcium Storage
Barium Sulfate (Barite)	$BaSO_4$	Gravity Device
Silicon Dioxide (Silica)	SiO_2	Algae Exoskeleton
Iron Oxide (Magnetite)	Fe_3O_4	Magnetotaxis
Ferrihydrite	$5Fe_2O_3.9H_2O$	Iron Storage

Nucleation is the initial phase transition where ions, atoms or molecules started to aggreagate and form a crystal in a solution, liquid or vapour. This process is essential in biomineralization since initiates the formation of a new thermodynamic phase in a controlled and regulated manner within the organix matrix (Vekilov 2010). Furthermore, controlled nucleation helps in producing uniform and well-ordered crystals, which are essential for the mechanical properties of the mineralized tissue. There are three theories explaining the deposition of inorganic solis (Gebauer et al. 2018; De Yoreo et al. 2015; Dubrovskii 2014):

Classical Nucleation Theory (CNT) was proposed in the 1930s and is the most commonly employed theory for quantitatively studying how higher-order assemblies are formed and controlled by kinetic and thermodynamic variables (Gebauer et al. 2018; Schmelzer 2010; Dubrovskii 2014). There are three keys aspects involved in CNT: Gibbs Free Energy (ΔG), Critical Size and Nucleation Rate (J). CNT defines nucleation is a competition between the decrease in free energy caused by the formation of a more stable phase and the increase in free energy caused by the formation of an interface between the newly formed phase and metastable phase. The overall free energy change demanded to produce a nucleus is calculated by the sum of these two effects. The critical size is the threshold where the free energy change for nucleation reaches its maximum level. When nuclei are lower than critical size, they become unstable and disintegrate, whereas larger nuclei can expand steadily. The nucleation rate refers to how quickly nuclei form in a system and becomes affected by parameters involving the supersaturation level,

temperature and nucleus surface energy. Since this theory relies on the motion of critical nuclei serving as transition states in supersaturated solutions, it requires higher energy during the nucleation (Schmelzer 2010).

Non-Classical Nucleation Theory: Researchers discovered that the phase transition does not directly resulted with the formation of the thermodynamically stable phase; instead, it may pass through intermediate phases with higher free energies rather lower nucleation barriers (Figure 1.2.)(Gebauer et al. 2018; Orava and Greer 2017; Schmelzer 2010; Dubrovskii 2014). Even complex materials such as proteins, minerals and polymeric solutions possess this behavior (Addadi and Weiner 2014; Sharma et al. 2021). For example, calcium phosphate mineral undergoes various phase transformations including hydroxyapatite (HAp), β-tricalcium phosphate (β-TCP), α-tricalcium phosphate (α-TCP), octacalcium phosphate (OCP), monocalcium phosphate (MCP) or amorphous calcium phosphate (ACP) depending on temperature, pH and ion concentration variables (Dogan et al. 2018a). Therefore, the second model, non-classical nucleation theory was developed to address limitations while CNT cannot entirely explain (Orava and Greer 2017). Therefore, the second model, Non-Classical Nucleation Theory noted the presence of pre-nucleation clusters during initial stage which are further assimilated to form amorphous mineral phases. The amorphous mineral phases are then converted into high-ordered crystal aggregates (Gebauer et al. 2018).

Crystallization by particle attachment (CPA) is a well-known phenomenon that describes how crystals form upon interactions with ion clusters, gels or oligomers and aggregate. Conceptually, it combines classical and non-classical theories. CPA theory has gained traction within several fields including mineralogy, materials science and biochemistry due to its ability to explain a wide range of natural and synthetic processes (De Yoreo et al. 2015). Since this nucleation theory is applicable within the biomineralization process, it will be utilized in directing the selection of mineralizing peptides throughout this thesis.

Once nucleation has occurred, crystal growth proceeds through the addition of more ions to the mineral structure (Figure 1.3.). The organic matrix and other regulatory molecules can govern the rate and direction of crystal formation ensuring the mineral forms in proper shape and size (Dubrovskii 2014; Vekilov 2010; Sharma et al. 2021).

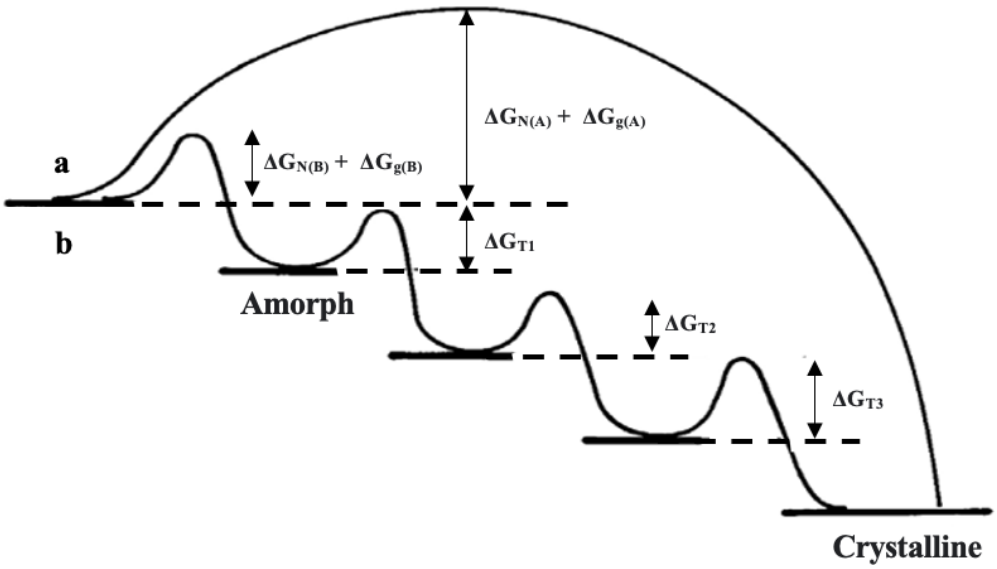

Figure 1.2. (a) Classical Nucleation vs (b) Non-Classical Nucleation Theory.

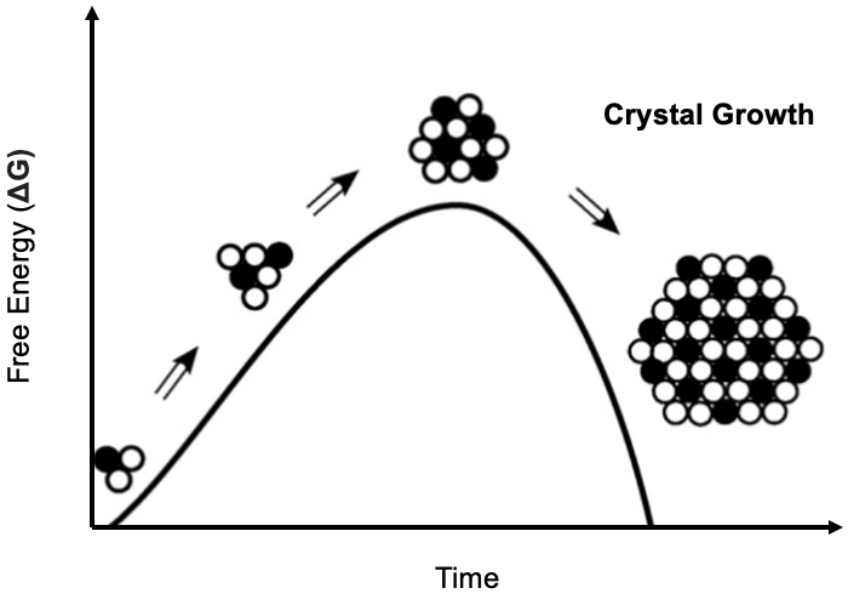

Figure 1.3. Crystal Growth.

Following crystal growth, the mineral structure may undergo successive modifications as cellular activity remodeling of the mineral phase (as in bone) or the addition of organic/inorganic layers achieving the desired eventual characteristics (Addadi and Weiner 2014; Dubrovskii 2014; Vekilov 2010; Sharma et al. 2021).

1.2. Importance of Biomineralization in Health and Effect on Well Being

Biomineralization serves an essential role in health and well-being by regulating the formation of minerals in biological hard tissues (Dorozhkin and Epple 2002). Regulating calcium/phosphate mineral in bone and teeth is vital for maintaning mineral production, structure, strength, integrity and mobility (Dorozhkin and Epple 2002; Cai and Tang 2008; Dorozhkin 2011). Beyond bones and teeth, it additionally serves to strengthen tendons and accumulate minerals for certain types of cartilage. Although it is a major biological process necessary to sustain life, dysregulation may lead to significant health issues (Sozen, Ozisik, and Calik Basaran 2017; Goldbourt and Neufeld 1986). Abnormal mineral deposition (calcium and pyrophosphate) can cause disorders like arthritis, in which crystals accumulate in the joints causing pain and inflammation. In vascular diseases, calcium deposits in the walls of arteries may stiffen blood vessels resulting in arteriosclerosis and decreased blood flow, developing the risk of high blood pressure, heart attack, and stroke (Goldbourt and Neufeld 1986). Kidney stones are another kind of pathological biomineralization; when minerals crystallize and form stones within the kidneys or urinary tract, causing considerable discomfort and obstruction. Furthermore, a reduction in bone mineral density increases the risk of fracture and causes osteoporosis (Sozen, Ozisik, and Calik Basaran 2017). Last but not least, inappropriate biomineralization may result in a number of dental illnesses including dental caries, dental fluorosis, tooth erosion and periodontitis (Petersen et al. 2005a). With regard to these consequences, understanding the mechanisms of biomineralization become crucial for developing treatments associated with abnormal mineral deposition diseases.

1.3. Dental Diseases Associated with Mineralization (Demineralization)

Oral and dental health is essential regarding our overall health and well-being and its deterioration has a detrimental impact on human health and quality of life (Sheiham 2005). As an instance, oral and dental-related problems have been attributed to an increased risk of cardiovascular illness, chronic lung disease, stomach and intestinal disease, high blood pressure, osteoporosis, diabetes and premature birth (Haque, Sartelli, and Haque 2019; Petersen et al. 2005a). According to the World Health Organization, tooth decay and gingivitis are among the most frequent disorders (Haque, Sartelli, and

Haque 2019; Petersen et al. 2005; Baelum et al. 2007). In the 19th and 20th centuries, it was classified as a worldwide epidemic and still it's the most prevalent secondary health problem in the world. 60-90% of today's school-age children and almost 100% of adults have at least one tooth decay (Haque, Sartelli, and Haque 2019; Carvalho and Schiffner 2019). Although high-income countries have reduced the incidence of dental decay in the last 30 years, it remains the most frequent disease in middle- and low-income countries, negatively affecting public health (Haque, Sartelli, and Haque 2019; Petersen et al. 2005b; Pitts et al. 2017). Though high-income countries had a 53% prevalence of treated tooth caries in children aged 11-14, low-income countries have a rate of around 2% (Listl et al. 2015). As an outcome, tooth decay is not only a malnutrition-related disease, nevertheless also a social deprivation-related disease.

Oral and dental diseases have been classified as white spot lesions, dentin hypersensitivity, dental cavities, root decay, gingivitis, periodontitis etc. (Figure 1.4.) (Cheng et al. 2009; Moynihan and Petersen 2004; Baelum et al. 2007). White spot lesions are opacities that occurred by demineralization of enamel under the surface (Bishara and Ostby 2008). Dentin hypersensitivity occurs when dentin tubules become exposed due to loss of protective enamel and cementum tissues (Varoni et al. 2017; Yang et al. 2016)(Varoni et al. 2017; Yang et al. 2016). Dental caries is a chronic diseases caused by bacterial biofilm on a tooth surface that has been exposed to fermentable carbohydrate substrates over time, resulting in demineralization and eventually cavitation (Jensen 1999; Touger-Decker and van Loveren 2003). Gingitivis is gum that commonly occurs whener plaque or bacteria accumulates on the teeth; if untreated, it can develop into periodontitis. In this case, inflammation spreads from the gums (gingiva) to the ligaments and bone which hold up the teeth. This is more serious and may result in tooth loss (Lang, Schätzle, and Löe 2009).

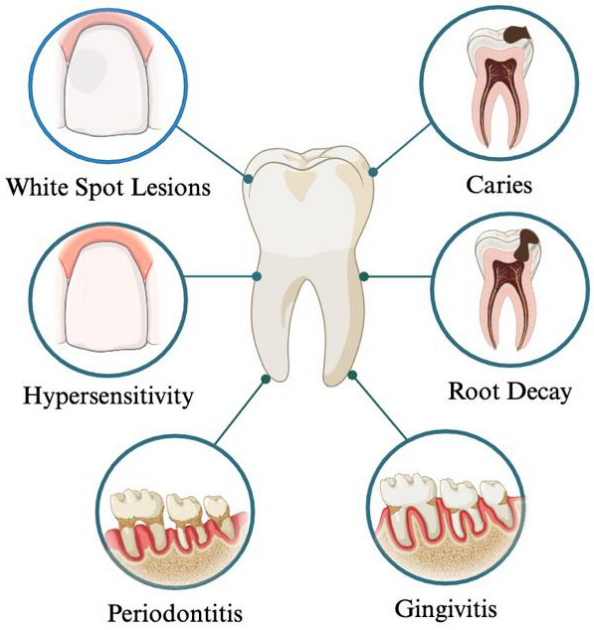

Figure 1.4. Common Dental Diseases.

There are many factors that contribute to oral health degradation. These causes include inadequate dental brushing habits, the consumption of sugary food and drinks, the use of medications that inhibit saliva secretion in the mouth (Moynihan and Petersen 2004; Pitts et al. 2017). Nonetheless, the primary contributing factor for the development of oral and dental degradation is the erosion of the minerals that comprise dental tissue in response to acidic attack and mechanical wear (Buzalaf, Hannas, and Kato 2012).

1.3.1. Dental Tissues and Mechanism of Demineralization

Teeth are composed of four dental tissues (Tjäderhane et al., n.d.; Beniash et al. 2019) . Three of these are hard tissues: enamel, dentin, and cementum; the fourth is the pulp, which is located in the core of the tooth and contains nerves, blood vessels and connective tissue; it is a soft, non-calcified tissue. It is apparent that hard tissues of the teeth are highly made of hydroxyapatite (HAp) minerals (Table 1.2.) (Gil-Bona and Bidlack 2020; Lyngstadaas et al., n.d.; Beniash et al. 2019).

Table 1.2. Dental Hard Tissues Composition;

Enamel	~ 95-98% HAp, 3% organic matter and water
Dentin	~70% HAp, 30% organic matter, collagen and water
Cementum	~ 45% HAp, 55% organic matter, collagen and water

Demineralization is the loss of minerals from tooth hard tissues triggered by bacterial acid attack and mechanical wear (Neel et al. 2016). It is generally caused by the interaction of bacteria in the mouth which breaks down carbohydrates (e.g., glucose, sucrose, or fructose) and creates an acidic environment (Figure 1.5.) (Dodds, Hsieh, and Johnson 1991; Kleinberg and Jenkins, n.d.). This environment results in mineral loss from the dental tissues (Neel et al. 2016). Although saliva secreted in a healthy mouth can reverse daily mineral loss, erosion caused by carbohydrate-containing foods and drinks inhibits the minerals (calcium, phosphate) brought back by saliva (Jensen 1999; Buzalaf, Hannas, and Kato 2012; Abelson and Mandel 1981). Furthermore, poor dental hygiene and a diet in sugary foods and beverages promote the growth of acid-producing bacteria (*Streptococcus mutans and Streptococcus sorbrinus*) (Touger-Decker and van Loveren 2003; Jensen 1999). These bacteria reduce the pH of the oral flora making the salivary environment more acidic (Dodds, Hsieh, and Johnson 1991; Marshall et al. 1997a). Once these bacteria reach the surface enamel, the acids they released dissolve the hydroxyapatite mineral in the tooth enamel resulting in the demineralization of the enamel layer (Neel et al. 2016). Due to the non-regenerative nature of the enamel layer, it cannot renew and repair itself after demineralization, causing tooth decay (Neel et al. 2016; Gil-Bona and Bidlack 2020). If tooth decay is not treated for a long time, the decay can reach to the nerves and infect the tooth, causing an abscess that can cause severe pain, facial swelling and fever (Buzalaf, Hannas, and Kato 2012; Cheng et al. 2009). If there is no intervention in the later stages, the resulting situation necessitates root canal therapy or tooth extraction. Dental diseases due to demineralization can be classified as dental caries, white spot lesions, dentin hypersensitivity and gingivitis (Neel et al. 2016; Marshall et al. 1997b). Globally, dental diseases resulting from demineralization impose a huge financial burden on patients, amounting to approximately $300 billion annually (Listl et al. 2015).

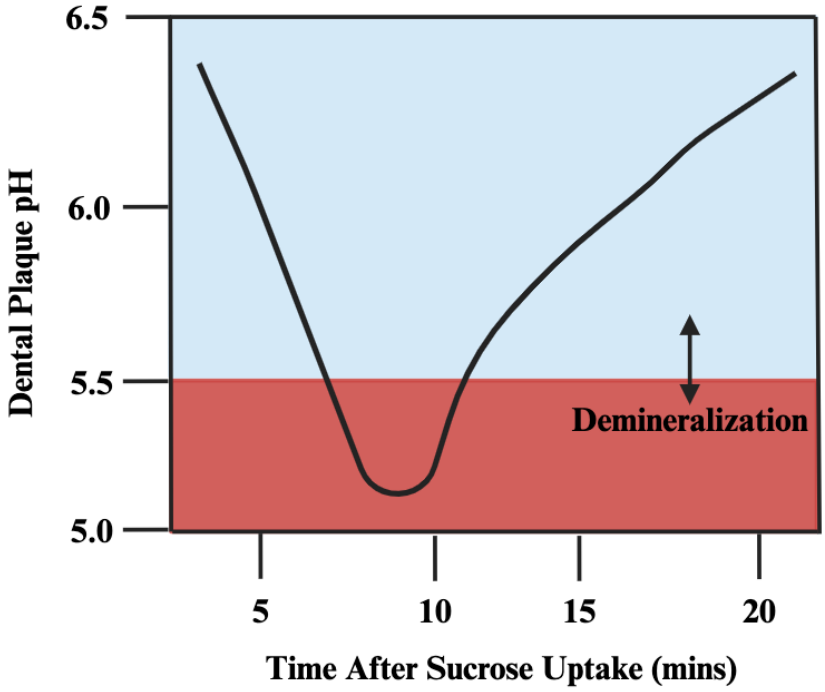

Figure 1.5. Mechanism of Demineralization in Response to Sugar Uptake.

1.3.2. Current Treatments and Issues

There are current treatments commonly used in dental clinics including fluoride treatment, dental fillings and dental implants. Despite the fact that these standard clinical approaches have been utilized for over sixty years; they have some substantial limitations.

Fluoride therapy is used to assist eliminating tooth decay by strengthening tooth enamel while making it more resistant to bacterial acid attack (Gao et al. 2016; Beltrán-Aguilar, Goldstein, and Lockwood 2000). While fluoride is delivered to the tooth surface through a carrier substance such as toothpaste or gel, fluoride ions interact with saliva and available calcium ions on the tooth surface and generate calcium fluoride which accumulates on the surface nonspecifically (Dogan et al. 2018b). Due to the incompatibility between the dental tissue mineral (HAp) and generated calcium fluoride particles, this created barrier against demineralization is temporary (Dogan et al. 2018b). Fluoride, on the other hand, is a neurotoxin that can be dangerous while taking in high doses and excessive usage can damage the bones and the joints, leading to dental or skeletal fluorosis (Kashyap, Sankannavar, and Madhu 2021).

Once amalgam or composite based fillers are applied to a cavitated surface, they creat a gap at the tissue-restrotative material interface, which provides a protected environment for bacteria to penetrate and continiue to grow (Peutzfeldt et al. 2018; Bernardo et al. 2007). These serve as secondary cavitation surfaces and cavitation becomes even more serious. Nevertheless, due to physical (crystallography, morphology) and chemical differences (elemental compositions and phases) from the native teeth structure, the dental materials utilized are incompatible with biological tissues at the lesion-restorative material interaction (Dogan et al. 2018b).

In the case of dental implants, although titanium has very superior characteristic material proporties such as osteointegration, success rate of dental implants are still low and often failed due to the implant infections (Pye et al. 2009).

1.3.3. Current Approaches and Limitations

Due to the concerns with current treatment methods, there are several approaches have been conducted on mimicking biological processes of oral environment to avoid or reconstruct mineral loss from dental hard tissues, enamel, dentin and cementum, which could further lead to demineralization-related diseases as white spot lesions, cavities, hypersensitivity and deep-root cavities (Niu et al. 2014; Kwak et al. 2017; Chien et al. 2017; Kim et al., n.d.). These researches encompass whole proteins and protein fragments (Amelogenin), Bioactive Glass (Novamin), CPP-ACP (MI Paste) and Polymers (Fan, Sun, and Moradian-Oldak 2009a; Vollenweider et al. 2007; D. Wu et al. 2013; Figueiredo Macedo de Lima et al. 2020; Chien et al. 2017).

Proteins have a crucial role in constructing and coordinating solid components in biological hard tissues resulting in complex and functional structures (Oren et al. 2007). Dental tissue spesific proteins have been identified over the last quarter century and the fundamental functions of these proteins in forming minerals have been revealed. Amelogenin is a low molecular weight protein that is involved in the formation of enamel and tends to build the hardest and most mineralized tissue in the human body through controlling the dimension and directionality of HAp crystals, $Ca_{10}(PO_4)_6(OH)_2$, within the assembled protein matrix (Paine et al. 2001; Gungormus et al. 2012a; Dogan et al. 2018b). Therefore, Amelogenin and other extracellular matrix proteins e.g. enamelin, tuftelin, dentin sialoprotein, cementum attachment protein stand out as

effective agents for treating demineralization related issues (El Gezawi et al. 2019; Niu et al. 2014; Ruan et al. 2013; Jeremias et al. 2013; Fan, Sun, and Moradian-Oldak 2009b). Considering recent protein and protein fragments based approaches, the usage of these proteins was avoided due to their limited intra-oral stability and detection and deactivation by available proteases in saliva (Gungormus et al. 2012a; Dogan et al. 2018b). Furthermore, extracellular matrix proteins have a number of biochemical functions and each function are carried out by extremely small functional domains (active domains) within the proteins which are insufficient to regulate mineral synthesis (Oren et al. 2007; D. T. Yucesoy et al. 2018).

In principle, Bioactive Glass (Novamin) and MI Paste mimics the action of the saliva by utilizing the calcium and phosphate ions into the environment; nevertheless, these procedures rely on increasing the apitaxial mineralization on the surface of the tooth with no control on catalytic rate, morphology and composition (Vollenweider et al. 2007; D. Wu et al. 2013; Figueiredo Macedo de Lima et al. 2020). Furthermore, although these materials are utilized in dental care due to their ability to promote remineralization, the process of ion release and subsequent remineralization is extremely slow (Ca^{+2} consumption rate of Bioglass: 0.03 ng/min; Ca^{+2} consumption rate of Novamin: 0.02 ng/min) and requires prolonged exposure to provide substantial results(Arshad, Zaidi, and Farooqui 2021; Reddy et al. 2019; Peitl, Dutra Zanotto, and Hench, n.d.) . Meanwhile, the pH of the oral environment, e.g. acidic conditions in dental caries, influence their efficicacy on ion release and bioactivity proporties (Vollenweider et al. 2007).

Recently, polymers e.g., casein phosphopeptides, polymer induced-liquid precursors (PILP), amphiphilic peptoids and peptide like polymers consisting N-substituted glycines, are of especially interest for researchers focusing to improve the natural repairing processes of the teeth (Burwell et al. 2012; Chien et al. 2017; Kirkham et al., n.d.). Although polymers provide unique techniques for remineralization, they have severe limitations as biocompatibility difficulties, limited longevity, insufficient remineralization depth and controlling releasing rates (Chien et al. 2017). It may degrade over time in the oral environment due to mechanical forces with the presence of saliva, enzymes and bacterial activity and this limits the duration of its effectiveness while promoting remineralization (Chien et al. 2017). Although it can aid in forming mineral, the extent, organization and interaction of the HAp crystals is inadequate for complete recovery of structure and function (Burwell et al. 2012; Chien et al. 2017).

1.4. Synthetic Synthesis Methods of Ca/P Mineral

Hydroxyapatite (HAp), $Ca_{10}(PO_4)_6(OH)_2$, is a naturally occurring mineral form of calcium apatite with the hydroxide ion occupying the phosphate group (Read 1970; Addadi and Weiner 2014). Since it is the primary component of teeth and bone mineral, as well as an essential material in many biological and synthetic applications due to its high biocompatibility and bioactivity, the synthesis of Hap have long been inspired by material scientists and engineers (Szcześ, Hołysz, and Chibowski 2017). It can be synthetically synthesized utilizing a variety of processes including dry methods, wet methods and high-temperature methods (Figure 1.6.) (Shojai et al. 2013; Mohd Pu'ad et al. 2019). These synthesis methods attempt to produce HAp particles with controlled size, purity and crystallinity which are crucial for its applications e.g., in drug delivery, hard tissue engineering and implant coatings, etc (Sadat-Shojai et al. 2013).

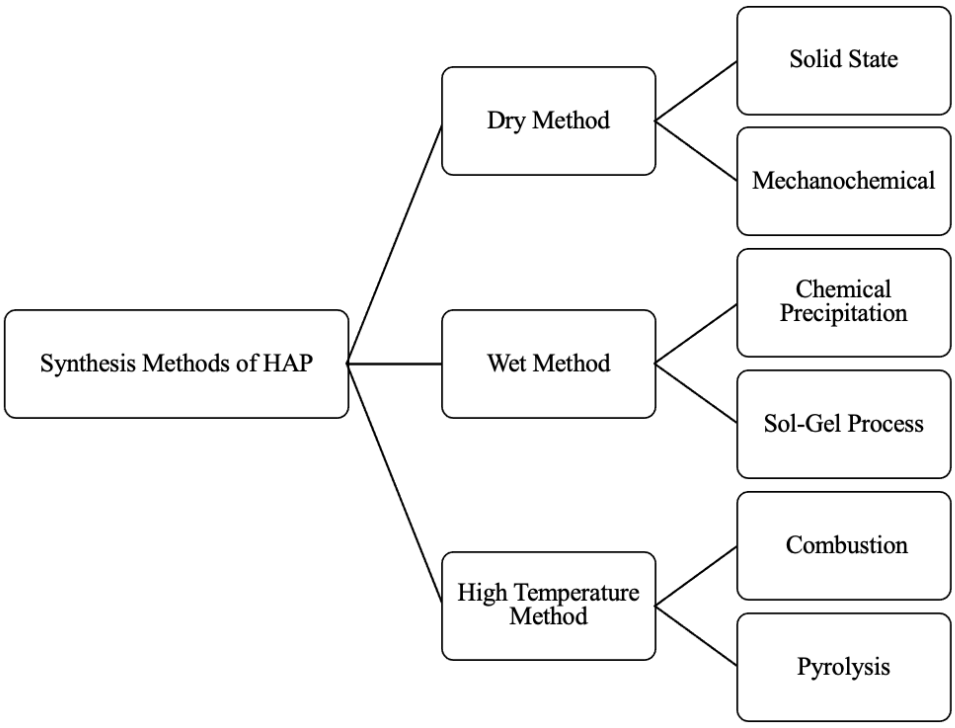

Figure 1.6. Synthetic Synthesis Methods of HAp.

1.4.1. Dry Synthesis Methods

Dry synthesis methods for HAp use methodologies that do not require a liquid media or substantial drying or calcination stages to remove water and are categorized into two types: solid-state and mechanochemical methods (Fahami, Ebrahimi-Kahrizsangi, and Nasiri-Tabrizi 2011; Pramanik et al. 2007).

Solid-State Method: This process involves the direct reaction of solid precursors, generally calcium phosphate, calcium carbonate or calcium oxide at high temperatures. Basically, the mixture is heated in furnace upon high temperatures (often above 1000°C) to facilitate the reaction for leading hydroxyapatite formation (Teshima et al. 2009; Taş 2001; Pramanik et al. 2007).

Mechanochemical Method: This method employs mechanical energy to stimulate chemical reactions between the precursors. It entails grinding/milling solid reactants (calcium phosphate or calcium hydroxide) under dry conditions and mechanical force induces the reaction to generate HAp at room temperature (25-27°C) (Silva et al. 2007; Nasiri-Tabrizi et al. 2009; Mochales et al. 2011; Fahami, Ebrahimi-Kahrizsangi, and Nasiri-Tabrizi 2011).

Calcination at a relatively high temperatures or high rotating speeds not only leads to phase transformations and the loss of hydroxide groups affecting the purity of HAp but also offers less control over the particle shape and surface morphology. Therefore, HAp particles synthesized via dry methods are irregular in shape, have low phase purity and non-stoichiometric (Table 1.3.) (Silva et al. 2007; Nasiri-Tabrizi et al. 2009; Mochales et al. 2011; Fahami, Ebrahimi-Kahrizsangi, and Nasiri-Tabrizi 2011; Teshima et al. 2009; Taş 2001; Pramanik et al. 2007).

Table 1.3. Characteristics of HAp synthesized via Dry Methods;

	Characteristics of Powder				
Dry Methods	Morphology	Crystallinity	Phase Purity	Ca/P Ratio	Size
Solid-State Method	Diverse	High	Low	Variable	Micron
Mechanochemical Method	Diverse	High	Low	Non-stoichiometric	Nano

1.4.2 Wet Synthesis Methods

Wet synthesis methods utilize chemical reactions in a liquid media under relatively mild conditions. The most prevalent wet synthesis procedures are chemical precipitation and the sol-gel methods (Ramanan and Venkatesh 2004; Ikoma et al. 1999).

Precipitation Method: This is one of the simplest and extensively used procedure for synthesizing hydroxyapatite. It entails combining aqueous calcium and phosphate solutions over specific pH and temperature. Basically, the HAp precipitates out of the solution and is filtered, rinsed and dried (Ikoma et al. 1999; Zhan et al. 2005; Silva et al. 2007).

Sol-Gel Method: This process involves the transition of a system from a liquid "sol" (a colloidal suspension of particles) to a solid "gel" phase. Precursors, alkoxides or metal salts, undergo hydrolysis and polycondensation resulting in a gel-like network with liquid and solid components. After drying and calcination, the gel is transformed into HAp (Ramanan and Venkatesh 2004; D. W. Kim et al. 2010).

Although these methods enables the production of HAp with high purity and uniform particle size, the resulting synthesized particles are often amorphous and require further heat treatment in order to achieve the desired crystallinity (Ramanan and Venkatesh 2004; D. W. Kim et al. 2010; Ikoma et al. 1999; Zhan et al. 2005; Silva et al. 2007).

1.4.3 High-Temperature Synthetis Methods

High-temperature synthesis methods (e.g., combustion, pyrolysis) for hydroxyapatite involve chemical reactions that usually takes place at temperatures above 800°C (An et al. 2007; Cho and Kang 2008). At these temperatures, there is a potential of creating HAp with lower phase purities (e.g., octacalcium phosphate (OCP), monocalcium phosphate (MCP), dicalcium phosphate (DCP), β-tricalcium phosphate (β-TCP) or tricalcium phosphate (TCP)) and it may provide less control over the microstructure of HAp than lower-temperature methods (Dogan et al. 2018b; D. T. Yucesoy et al. 2018). These limitations may have an adverse impact on the material's performance in specific applications notably those requiring surface area properties or pore sizes (Scalera et al. 2013). Furthermore, high-temperature processes require significant energy input, making them less energy-efficient and potentially more expensive than low-temperature synthesis techniques (Sadat-Shojai et al. 2013; Mohd Pu'ad et al. 2019).

In brief, although each synthesis method has its advantages and chosen based on the specific requirements of the application, the limitations (morphology, particle size, phase purity, crystallinity) mentioned above need to be addressed. Last but not least, since saliva in the mouth has an average pH at 6.7 and oral temperature is roughlty at 37°C, these three methods of HAp synthesis are inappropriate for biological conditions (Leong Lim, Byrne, and Lee 2008; Sadat-Shojai et al. 2013).

1.5. Biomimetic Synthesis Methods of Ca/P Mineral

The utility of combinatorially selected peptides through viral- or bacterial-displayed peptide libraries have been proven to be a promising approach for identifying peptide sequences that have specific affinities to a variety of inorganic surfaces (Deniz Tanil Yucesoy et al. 2015; Deniz T. Yucesoy et al. 2015, 2020; Tamerler and Sarikaya 2007; Zin et al. 2005; Rath et al., n.d.; D. M. Fowler and Fields 2014). In this approach, researchers used combinatorial expression technique to identify hydroxyapatite binding peptides (HABPs) resulting in a set of sequences that could offer controlling calcium phosphate-based biomineral formation (Gungormus et al. 2008). This study focused on screening of a cysteine-constrained M13 bacteriophage heptapeptide library against

hydroxyapatite powder. They've selected more than 50 sequences to demonstrate their binding affinities and structural properties on calcium phosphate (Ca/P) mineralization. Two sequences were identified, one that exhibited the highest binding affinity (HABP1) and the other, a much lower binding affinity (HABP2) to HAp. The identified peptides have been proven to alter mineralization activity and form significantly larger crystals in the presence of HABP1 and HABP2 than the negative control.

In another study, researchers aimed to describe a novel protocol for identifying peptide sequences from native proteins that have potential to repair damaged dental tissues by regulating hydroxyapatite biomineralization (Gungormus et al. 2012a). The advantage of identifying peptides was that they can escape from oral proteases as well as other immune system components, and they are easy to control and produce. For this purpose, amelogenin (involved in the formation of enamel) was utilized as a case study and a bioinformatics scoring matrix, and researchers have identified regions within amelogenin that are shared with a set of hydroxyapatite-binding peptides (HABPs) previously selected by phage display. Using the bioinformatics matrix, distinct peptide domains within the 180 amino acid amelogenin protein (rM180) were previously discovered as being comparable to a set of 155 HAp-binding peptide (HABP) sequences determined using 7-AA and 12-AA phage display libraries. In the same study, Amelogenin-Derived Peptide 5 (ADP5), a 22 amino acid long peptide sequence, stimulates the cell-free formation of a cementum-like hydroxyapatite mineral layer on human root dentin, thereby enhancing periodontal ligament cell attachment.

Researchers demonstrated further studies utilizing biomimetic restoration of artificially demineralized human enamel and dentin through peptide-guided remineralization approach. As an outcome, ADP5 resulted in the formation of a very thick, densely mineralized layer on demineralized enamel that resembles the structure of healthy enamel and contains HAp mineral (Dogan et al. 2018b). Furthermore, employing the mineralization directing peptide, ADP5, the occlusion was accomplished layer by layer through peptide-guided remineralization process intruding mineral layer on exposed dentin tubules (Deniz T. Yucesoy et al. 2023).

These conducted studies have been employed traditional directed evolution method and bioinformatic methodology primarily focusing on achieving the remineralization of enamel drawing inspiration from the amelogenin protein; however, if dental anatomy was examined, it exposes different various hard and soft tissues within the tooth structure including dentin, cementum and pulp. On the other hand, the selection

of identified peptides was primarily focused binding affinities to HAp mineral followed by an assessment of their mineralization abilities. When calculated the reactions kinetics of these identified peptides within this approach by their Ca+2 consumption rates were quantified as 0.0005 ng/min, 0.0015 ng/min and 0.0033 ng/min for HABP1, HABP2 and ADP5, respectively. Although these peptides were utilized in remineralization methodologies due to their ability to promote HAp mineralization, the process of ion release and subsequent remineralization was slow. Moreover, this approach was time-consuming and costly. Therefore, it arises a need for more targeted and expeditious methodology to address these challenges.

1.6. Goal of the Thesis

The intended objective of this thesis was to identify novel short mineralization catalyzing peptides that can govern hydroxyapatite mineralization and exhibit fast mineral formation rate in an aqueous media similar to natural proteins with directed evolution. The primary reason lay in identification of short peptide sequences was their potential to escape from immune cells and protease enzymes within the oral environment; at the same time, these short sequences facilitate ease of control and production rendering them advantageous for therapeutic applications. The criterion success of identifying peptides with inherent catalytic capabilities that directly induce mineralization was facilitating mineral formation rate faster than the state of art. Owing to the obtained success criteria, it was envisaged that these peptide sequences could serve as foundational elements in the development of clinical products as dental gels and toothpaste formulations in order to restore the remineralization abilities of dental tissues that have been subjected to acidic and mechanical erosion attack. These products which will prevent mineral loss in tissues could enable sustainable tissue regeneration and reduce the consumption of synthetic material-based restorative treatments. Moreover, the identified peptide sequences could extend in potential to restore demineralized tissues and treating diseases related to pathological mineralization.

CHAPTER 2

MATERIALS & METHOD

The intended objective of this thesis was to identify novel short mineralization catalyzing peptides that can guide HAp mineralization similar to natural proteins by directed evolution. Initially, the effect ion concentration on Ca/P Mineralization was optimized for identifying mineralizing peptides. After that, mineralization catalyzing peptides were chosen utilizing a directed evolution through M13 Phage Display Library (Ph.D. Phage Display Library, New England BioLabs Inc., USA). Once the mineralizing peptides were selected, their DNAs were extracted using QIAprep Spin M13 Kit (QIAGEN, Germany) and sequenced utilizing sanger-sequencing approach with an Applied Biosystems Genetic Analyzer (HITACHI, Germany). Subsequent mineral formation rates of the peptides were monitored by continious measuring of absorbance at 820 nm wavelength using a UV-Spectrophotometer (Thermo Fisher Scientific, USA). Simultaneously, the kinetic rate ability of the peptides was calculated by quantifying calcium concentration with Inductively Coupled Plasma Optical Emission Spectroscopy (ICP-OES). The structural analysis of the peptides with the highest mineral formation rate were observed by high-throughput characterization methods as Fourier Transform Infrared Spectroscopy (FTIR) and X-ray Diffraction (XRD).

2.1. Effect of Ion Concentration on Homogenous Ca/P Mineralization

19.2 mM $CaCl_2.2H_2O$ (AFG BioScience, USA) (pH:7.0 25°C), 11.52 mM KH_2PO_4 (Sigma Aldrich,USA) (pH: 7.0 25°C) and 50 mM HEPES (Sigma Aldrich, USA) (pH: 7.0 25°C) solutions were prepared. 50 mM Hepes Buffer was prepared in an ultra-pure water; 19.2 mM $CaCl_2.2H_2O$ and 11.52 mM KH_2PO_4 were prepared in 50 mM Hepes Buffer. The pH values of solutions were adjusted by Orion Star A211 pH Meter in accordance with 25°C. The reactions were carried out in seven setups: (i) 100 µL Ca^{+2}, 100 µL PO_4^{-3} (Ca/P: 9.6/5.76 mM); (ii) 75 µL Ca^{+2}, 75 µL PO_4^{-3}, 50 µL Hepes (Ca/P:7.2/4.32 mM); (iii) 66 µL Ca^{+2}, 66 µL PO_4^{-3}, 66 µL Hepes (Ca/P: 6.38/3.83 mM); (iv) 50 µL Ca^{+2}, 50 µL PO_4^{-3}, 100 µL Hepes (Ca/P: 4.8/2.88 mM); (v) 37,5 µL Ca^{+2}, 37,5

µL PO_4^{-3}, 125 µL Hepes (Ca/P: 3.6/2.16 mM), (vi) 33 µL Ca^{+2}, 33 µL PO_4^{-3}, 132 µL Hepes (Ca/P: 3.16/1.9 mM) and (vii) 25 µL Ca^{+2}, 25 µL PO_4^{-3}, 150 µL Hepes (Ca/P: 2.4/1.44 mM). The mineralization kinetics was measured at 820 nm during 10 seconds per 2 hours with low-continious shaking by UV-Vis Spectrophotometer (ThermoFisher Scientific, USA.

2.2. Selection of Mineralizing Peptides via Directed Evolution

Mineralization catalyzing peptides were chosen utilizing a directed evolution method through M13 Phage Display Library (Ph.D. Phage Display Library, New England BioLabs Inc., USA). Phage display is a technique for selecting peptide or protein variations wherein a library of peptide or protein variants exists on the outside of a phage virion while the genetic material encoding each variant is expressed on the inside (Smith and Petrenko 1997; Pande, Szewczyk, and Grover 2010; C. H. Wu et al. 2016). It forms a physical link between each variant protein sequence and the DNA that encodes it; allowing for quick partitioning based on binding affinity to a certain target molecule via an in-vitro selection process known as Biopanning. In this study, biopanning was performed by incubating a library of phage-displayed peptides in a Ca/P/Hepes solution, washing away the non-functional phages and eluting the particularly mineralization catalyzing phages. The phage that has been eluted is subsequently amplified and subjected to additional amplification cycles in order to enrich the pool in favor of mineralizing sequences. This elution protocol was performed over four Biopanning Rounds.

2.2.1. Biopanning Round I

125 µl $CaCl_2.2H_2O$ (19.2 mM, pH: 7.0 at 25°C), 125 µl KH_2PO_4 (11.52 mM, pH: 7.0 at 25°C), 240 µl Hepes (50 mM, pH: 7.0 at 25°C) and 10 µl M13-Bacteriophage (Ph.D. Phage Display Library, New England BioLabs Inc., USA) were added in a 2 ml sterile microcentrifuge tube (Final Volume: 500 µl; Ca/P: 4.88/2.88 mM; $2x10^{11}$ pfu/ml) (Figure 2.1.). The solution was allowed to react in a shaking incubator for 17 hours at a speed of 150 rpm at 25°C. After 17 hours, the tube was centrifuged at 14K rpm for 10 minutes and supernatant, BP1-S1 (Biopanning Round I- Supernatant 1), was transferred

into a new 1.5 ml sterile centrifuge tube. A pellet of mineral and phage was dissolved in 1000 µl Glycine Buffer (0.2 M, pH: 2.17) and neutralized with 160 µl Trizma Base (0.91 M, pH: 9.13). 800 µl of dissolved and neutralized phage was incubated with 1:200 inoculation from O/N, yield early log-phase (OD_{600}: 0.01-0.05) for 4 hours shaking at 250 rpm at 37°C; remained 360 µl phage was labelled as BP1-M1 (Biopanning Round I Mineralizing Peptide). The amplified phage was isolated (purified) by polyethylene glycol (PEG) (%20; w/v PEG-800, 2.49 M NaCl) and tris-buffered saline (TBS) (50 mM Tris-HCl, 150 mM NaCl; pH: 7.2) precipitation and was labelled as BP1-M2 (Biopanning Round I Amplified & Purified Mineralizing Peptide). Subsequently, serial dilutions of BP1-S1 (to examine the concentration of the phages remained in the supernatant), BP1-M1 (to examine the concentration of phages after mineralization) and BP1-M2 (to examine the concentration of phages remained after amplification and purification) were carried out . 20 µl of each dilutions (10^5-10^7 for BP1-S1 and BP1-M1; 10^{10}-10^{12} for BP1-M2) were transferred into a 15 ml falcon tube containing 3 ml of top agar + 180 µl of a mid-log (OD_{600}: ~0.34) culture of ER2738; were plated on LB-Agar containing 5-bromo-4-chloro-3-indolyl-β-D-galactopyranoside (Xgal) & isopropyl-β-D-thiogalactopyranosid (IPTG) plates (LB Agar-IPTG-Xgal plates) and incubated O/N at 37°C (Figure 2.2.). 17 hours later, blue phaqe plaques were counted and phage concentrations were calculated in accordance with the equation given in Equation 2.1 (Eq. 2.1.). The concentration of BP1-M2 was also measured by Nanodrop 8000 (ThermoScientific, USA) using its Uv-Vis program having a range of 269-320 nm and calculated in accordance with the equation given in Equation 2.2 (Eq. 2.2.).

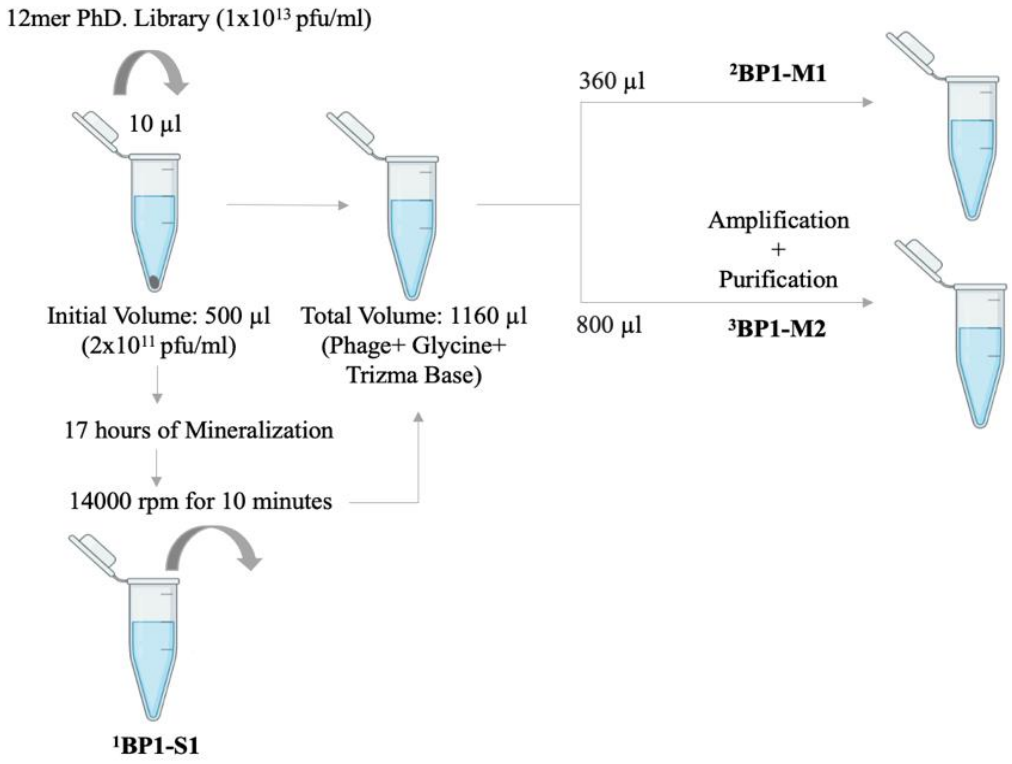

Figure 2.1. Biopanning Round I.

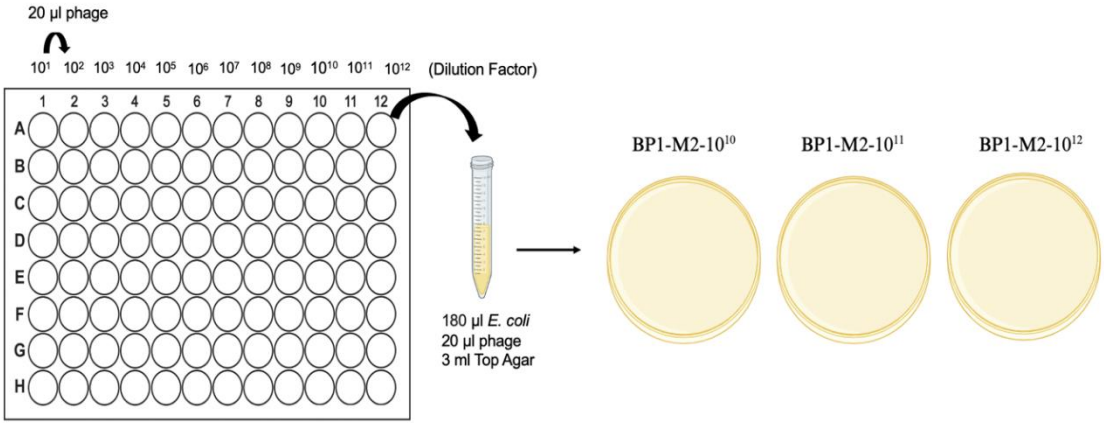

Figure 2.2. BP1-M2 Serial Dilution and Blue-White Colony Screening Process.

$$\#\text{of plaques} \times \text{dilution factor} \times \text{volume} \times \mu\text{l conversion} = \text{pfu/ml} \quad (2.1)$$

$$\frac{(A_{269}-A_{320}).\ 6\times10^{16}}{\text{number of bases}} = \text{virions/ml} \quad (2.2)$$

2.2.2. Biopanning Round II

In this round, BP1-M2 ($1x10^{13}$ pfu/ml) was used. 125 µl $CaCl_2.2H_2O$ (19.2 mM, pH: 7.0 at 25°C), 125 µl KH_2PO_4 (11.52 mM, pH: 7.0 at 25°C), 240 µl Hepes (50 mM, pH: 7.0 at 25°C) and 10 µl Phage were added in a 2 ml sterile microcentrifuge tube (Final Volume: 500 µl; Ca/P: 4.88/2.88 mM; $2x10^{11}$ pfu/ml) (Figure 2.3.). The solution was allowed to react in a shaking incubator for 17 hours at a speed of 150 rpm at 25°C. After 17 hours, the tube was centrifuged at 14K rpm for 10 minutes and supernatant, BP2-S1 (Biopanning Round II- Supernatant 1), was transferred into a new 1.5 ml sterile centrifuge tube. A pellet of mineral and phage was washed with 500 µl %0.01 detergent and dissolved for 5 minutes at a speed of 100 rpm at 25°C in an orbital shaker. The tube was spin down 14.000 rpm for 10 minutes and the supernatant was transferred into a new centrifuge tube and labelled as BP2-S2 (Biopanning Round II- Supernatant 2). Phage pellet was washed again with 500 µl %0.01 detergent and dissolved for 5 minutes at a speed of 100 rpm at 25°C in an orbital shaker and the supernatant was transferred into a new centrifuge tube and labelled as BP2-S3 (Biopanning Round II- Supernatant 3). Remaning pellet was dissolved in 1000 µl Glycine Buffer (0.2 M, pH: 2.17) and neutralized with 160 µl Trizma Base (0.91 M, pH: 9.13). 800 µl of dissolved and neutralized phage was incubated with 1:200 inoculation from O/N, yield early log-phase (OD_{600}: 0.01-0.05) for 4 hours shaking at 250 rpm at 37°C; remained 360 µl phage was labelled as BP2-M1 (Biopanning Round II Mineralizing Peptide). The amplified phage was purified by PEG (%20; w/v PEG-800, 2.49 M NaCl) and TBS (50 mM Tris-HCl, 150 mM NaCl; pH: 7.2) precipitation and was labelled as BP2-M2 (Biopanning Round II Amplified & Purified Mineralizing Peptide). Subsequently, serial dilutions of BP2-S1 (to examine the concentration of the phages remained in the supernatant), BP2-S2 (to examine the concentration of the phages after washed with %0.01 detergent), BP2-S3 (to examine the concentration of the phages after 2nd washed with %0.01 detergent), BP2-M1 (to examine the concentration of phages after mineralization) and BP2-M2 (to examine the concentration of phages remained after amplification and purification) were carried out . 20 µl of each dilutions (10^5-10^7 for BP2-S1, BP2-S2, BP2-S3 and BP2-M1; 10^{10}-10^{12} for BP2-M2) were transferred into a 15 ml falcon tube containing 3 ml of top agar + 180 µl of a mid-log (OD_{600}: ~0.34) culture of ER2738; were plated on LB Agar-IPTG-Xgal plates and incubated O/N at 37°C. 17 hours later, blue phaqe plaques were

counted and phage concentrations were calculated in accordance with the Eq. 2.1. The concentration of BP2-M2 was measured by Nanodrop 8000 using its Uv-Vis program having a range of 269-320 nm and calculated in accordance with the equation given in Eq. 2.2.

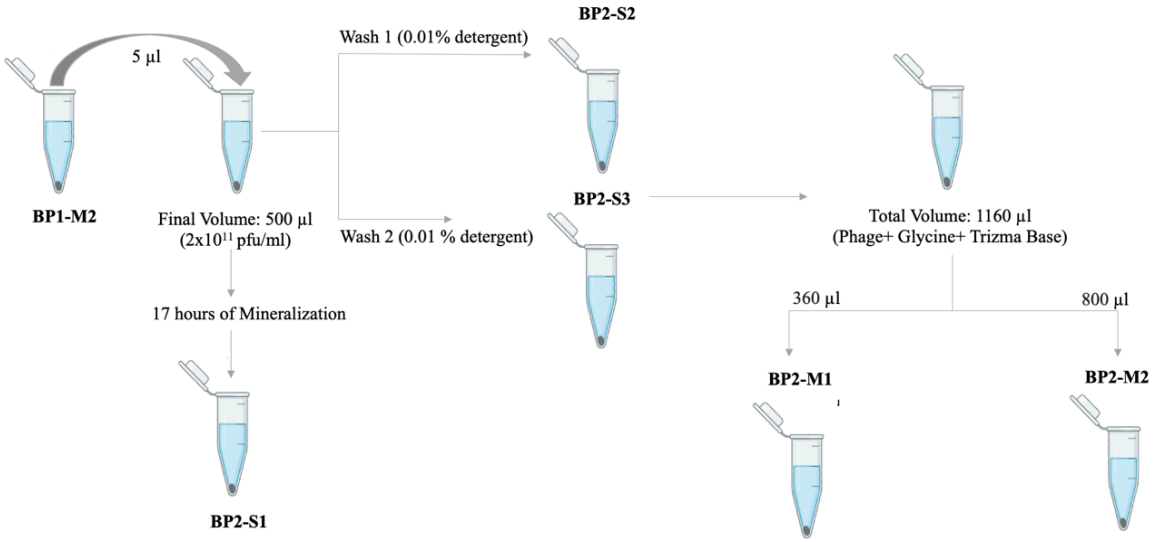

Figure 2.3. Biopanning Round II.

2.2.3. Biopanning Round III

In Biopanning Round III, BP2-M2 ($3{,}4x10^{13}$ pfu/ml) was used. 125 µl $CaCl_2.2H_2O$ (19.2 mM, pH: 7.0 at 25°C), 125 µl KH_2PO_4 (11.52 mM, pH: 7.0 at 25°C), 247 µl Hepes (50 mM, pH: 7.0 at 25°C) and 3 µl Phage were added in a 2 ml sterile microcentrifuge tube (Final Volume: 500 µl; Ca/P: 4.88/2.88 mM; $2x10^{11}$ pfu/ml). The solution was allowed to react in a shaking incubator for 17 hours at a speed of 150 rpm at 25°C. After 17 hours, the tube was centrifuged at 14K rpm for 10 minutes and supernatant, BP3-S1 (Biopanning Round III- Supernatant 1), was transferred into a new 1.5 ml sterile centrifuge tube. A pellet of mineral and phage was washed with 500 µl %0.01 detergent and dissolved for 5 minutes at a speed of 100 rpm at 25°C in an orbital shaker. The tube was spin down 14.000 rpm for 10 minutes and the supernatant was transferred into a new centrifuge tube and labelled as BP3-S2 (Biopanning Round III- Supernatant 2). Phage pellet was washed again with 500 µl %0.02 detergent and dissolved

for 5 minutes at a speed of 100 rpm at 25°C in an orbital shaker and the supernatant was transferred into a new centrifuge tube and labelled as BP3-S3 (Biopanning Round III-Supernatant 3). Remaning pellet was dissolved in 1000 µl Glycine Buffer (0.2 M, pH: 2.17) and neutralized with 160 µl Trizma Base (0.91 M, pH: 9.13). 800 µl of dissolved and neutralized phage was incubated with 1:200 inoculation from O/N, yield early log-phase (OD_{600}: 0.01-0.05) for 4 hours shaking at 250 rpm at 37°C; remained 360 µl phage was labelled as BP3-M1 (Biopanning Round III Mineralizing Peptide). The amplified phage was purified by PEG (%20; w/v PEG-800, 2.49 M NaCl) and TBS (50 mM Tris-HCl, 150 mM NaCl; pH: 7.2) precipitation and was labelled as BP3-M2 (Biopanning Round III Amplified & Purified Mineralizing Peptide). Subsequently, serial dilutions of BP3-S1 (to examine the concentration of the phages remained in the supernatant), BP3-S2 (to examine the concentration of the phages after washed with %0.01 detergent), BP3-S3 (to examine the concentration of the phages after 2nd washed with %0.02 detergent), BP3-M1 (to examine the concentration of phages after mineralization) and BP3-M2 (to examine the concentration of phages remained after amplification and purification) were carried out . 20 µl of each dilutions (10^5-10^7 for BP3-S1, BP3-S2, BP3-S3 and BP3-M1; 10^{10}-10^{12} for BP3-M2) were transferred into a 15 ml falcon tube containing 3 ml of top agar + 180 µl of a mid-log (OD_{600}: ~0.34) culture of ER2738; were plated on LB Agar-IPTG-Xgal plates and incubated O/N at 37°C. 17 hours later, blue phaqe plaques were counted and phage concentrations were calculated in accordance with the Eq. 2.1. The concentration of BP3-M2 was measured by Nanodrop 8000 using its Uv-Vis program having a range of 269-320 nm and calculated in accordance with the equation given in Eq. 2.2.

2.2.4. Biopanning Round IV

In Biopanning Round IV, BP3-M2 ($1x10^{13}$ pfu/ml) was used. 125 µl $CaCl_2.2H_2O$ (19.2 mM, pH: 7.0 at 25°C), 125 µl KH_2PO_4 (11.52 mM, pH: 7.0 at 25°C), 240 µl Hepes (50 mM, pH: 7.0 at 25°C) and 10 µl Phage were added in a 2 ml sterile microcentrifuge tube (Final Volume: 500 µl; Ca/P: 4.88/2.88 mM; $2x10^{11}$ pfu/ml). The solution was allowed to react in a shaking incubator for 17 hours at a speed of 150 rpm at 25°C. After 17 hours, the tube was centrifuged at 14K rpm for 10 minutes and supernatant, BP4-S1 (Biopanning Round IV- Supernatant 1), was transferred into a new 1.5 ml sterile

centrifuge tube. A pellet of mineral and phage was washed with 500 µl %0.01 detergent and dissolved for 5 minutes at a speed of 100 rpm at 25°C in an orbital shaker. The tube was spin down 14.000 rpm for 10 minutes and the supernatant was transferred into a new centrifuge tube and labelled as BP4-S2 (Biopanning Round IV- Supernatant 2). Phage pellet was washed again with 500 µl %0.05 detergent and dissolved for 5 minutes at a speed of 100 rpm at 25°C in an orbital shaker and the supernatant was transferred into a new centrifuge tube and labelled as BP4-S3 (Biopanning Round IV- Supernatant 3). Remaning pellet was dissolved in 1000 µl Glycine Buffer (0.2 M, pH: 2.17) and neutralized with 160 µl Trizma Base (0.91 M, pH: 9.13). 800 µl of dissolved and neutralized phage was incubated with 1:200 inoculation from O/N, yield early log-phase (OD_{600}: 0.01-0.05) for 4 hours shaking at 250 rpm at 37°C; remained 360 µl phage was labelled as BP4-M1 (Biopanning Round IV Mineralizing Peptide). The amplified phage was isolated was purified by PEG (%20; w/v PEG-800, 2.49 M NaCl) and TBS (50 mM Tris-HCl, 150 mM NaCl; pH: 7.2) precipitation and was labelled as BP4-M2 (Biopanning Round IV Amplified & Purified Mineralizing Peptide). Subsequently, serial dilutions of BP4-S1 (to examine the concentration of the phages remained in the supernatant), BP4-S2 (to examine the concentration of the phages after washed with %0.01 detergent), BP4-S3 (to examine the concentration of the phages after 2nd washed with %0.05 detergent), BP3-M1 (to examine the concentration of phages after mineralization) and BP4-M2 (to examine the concentration of phages remained after amplification and purification) were carried out . 20 µl of each dilutions (10^5-10^7 for BP4-S1, BP4-S2, BP4-S3 and BP4-M1; 10^{10}-10^{12} for BP4-M2) were transferred into a 15 ml falcon tube containing 3 ml of top agar + 180 µl of a mid-log (OD_{600}: ~0.34) culture of ER2738; were plated on LB Agar-IPTG-Xgal plates and incubated O/N at 37°C. 17 hours later, blue phaqe plaques were counted and phage concentrations were calculated in accordance with the Eq. 2.1. The concentration of BP4-M2 was measured by Nanodrop 8000 using its Uv-Vis program having a range of 269-320 nm and calculated in accordance with the equation given in Eq. 2.2.

2.2.5. Mineralization Analysis with Enrichment Libraries

19.2 mM $CaCl_2.2H_2O$ (pH: 7.0 25°C), 11.52 mM KH_2PO_4 (pH: 7.0 25°C) and 50 mM HEPES (pH: 7.0 25°C) solutions were used as mineralization reactants. Mineralization reactions for BP1-BP2-BP3-BP4-M2 were initiated with 10^{11} pfu in 200 µl (Final Concentration: $2x10^{11}$ pfu/ml; Ca/P: 4.8/2.88 mM) in a 96-well plate (Table 2.1). Mineral formation capability of identified libraries were monitored using a UV Spectrophotometer by continuous measuring of absorbance at 820 nm during 24 hours.

2.3. Selection of Peptides from Biopanning Round IV

BP4-M2 (amplified, purified) was serial diluted into 10^9 pfu that resulted ~80-100 peptides on LB Agar-IPTG-Xgal plate and mixed with 180 µl *E.Coli* culture (1:200 Inoculation from O/N yield mid log-phase, OD_{600}: ~0.34 in 4 hours). This mixture was transferred in 3 ml melt Top Agar and poured onto LB Agar/X-gal/IPTG-tetracycline plates. Agar plates was incubated at 37°C O/N. 17 hours later, 80 peptides were picked up by pipettor tip and put seperately into 150 µl of PC Buffer (0.02% detergent, pH: 7.2) in pre-sterilized 1.5 ml DNAse free centrifuge tubes. These tubes were shaken for 15 min at 150 rpm and incubated within Medisson Ultrasonic Bath at 60°C for 45 minutes and kept at 4°C for O/N. Next day, 150 µl of peptide solution, stored at 4°C, was transferred into 150 µl glycerol stocks (%50 glycerol) and was stored at -20°C.

2.4. ssDNA Isolation & Sequencing

Single-stranded (ssDNA) DNA was isolated using QIAprep Spin M13 Kit (QIAGEN, Germany). 10 µl of phage frozen glycerol stock (Biopanning Round IV-Selected Peptides) was added into 3 ml of *E.coli* culture ($OD_{early\text{-}midlog}$:~0.34) and incubated for 4 hours at 37 °C. Bacterial culture was spin down at 5000 rpm for 15 min at room temperature. Supernatant containing M13 bacteriophage was precipitated by incubating with 1/100 volume Buffer MP (M13 Precipitation Buffer; 2.86 M citric acid) for 2 minutes. After that, the samples were applied to the QIAprep spin columns and phage particles were retained specifically on the adapted silica membrane. Upon addition of Buffer PB (M13 lysis and binding buffer; 5 M Gu-HCl; %30 isopropanol), the phage

particles were lysed and single-stranded DNA was adsorbed to the membrane in the presence of high salt. In this way, contaminants such as phage proteins pass through and were eliminated. After a brief wash step with Buffer PE (10 mM Tris-HCl pH: 7.5; %80 ethanol), pure single-stranded DNA was eluted in 50 µl of Buffer EB (Elution Buffer; 10 mM Tris-HCl pH: 8.5) The concentration of the eluted DNAs was measured by Nanodrop 8000 (ThermoScientific, USA) using its nucleic acid program at 600 nm. The DNA sequencing of the peptides from BP4-M2 were sequenced with Sanger Sequencing method and had a two-stage process: spin colon preparation and cleaning, followed by cycle sequencing reactions.

2.4.1. Spin Colon Preparation and Cleaning

Sephadex colon was prepared in a falcon tube by mixing 1 g Sephadex G50 (Sigma Aldrich, USA) with 15 ml autoclaved ultra-pure water. After that, 650 µl of sephadex mixture was added to spin colons and waited for 10-30 minutes until seeing the phase separation in the tubes. Then tubes were centrifuged at 5400 rpm for 2 minutes. Top part was replaced into a new eppendorf tube as a clean elution tube without disturbing sephadex colon in it. PCR products (at least 10 µl) was pipetted on top of sephadex colon and were centrifuged at 5400 rpm for 2 minutes in order to collect clean PCR products.

2.4.2. Cycle Sequencing Reaction

The sequencing library is prepared by amplifying the 36 bp peptide-coding variable region. For sequencing, -96 gIII sequencing primer (Ph.D. Phage Display Libraries, New England BioLabs Inc., USA) was used. Cycle Sequencing Reaction was set as listed in Table 2.1.

-96 gIII sequencing primer: 5′- HOCCC TCA TAG TTA GCG TAA CG –3′, 1 pmol/µl

Table 2.1. Cycle Sequencing Reaction Setup;

Reagent	Volume (µl)	Concentration
Big Dye 3.1 RRM	1	1 pmol/µl stock (20 ng final)
5x Buffer	1.5	
Primer (-96 gIII)	1.6	
Template/water	5.9	
Total	10	

Thermal cycler program for Big Dye 3.1 cycle sequencing reactions was set up as follows:

1. Rapid thermal ramp to 96°C, hold for 1 minute
2. Rapid thermal ramp to 96°C, hold for 10 seconds
3. Rapid thermal ramp to 50°C, hold for 5 seconds
4. Rapid thermal ramp to 60°C, hold for 4 minutes
5. Back to step 2; 24 times (total of 25 cycles)
6. Rapid thermal ramp to 4°C, hold for 5 minutes

2.5. Peptide Amplification & Purification & Quantification

5 µl of frozen peptide/glycerol stocks (selected in Section 2.4.) from BP4-M2 were incubated with 1:200 inoculation from O/N yield early log-phase (OD_{600}: 0.01-0.05) for 4 hours shaking at 250 rpm at 37°C. The amplified peptides were isolated PEG and TBS buffer precipitation. Amplified & Purified peptide concentration was measured by Nanodrop 8000 (ThermoScientific, USA) using its Uv-Vis program having a range of 269-320 nm.

2.6. Mineralization Kinetic Analysis With Peptides

19.2 mM $CaCl_2.2H_2O$ (pH: 7.0 25°C), 11.52 mM KH_2PO_4 (pH: 7.0 25°C) and 50 mM HEPES (pH: 7.0 25°C) solutions were used as a mineralization reactants. Mineralization reactions for each peptide were initiated with 10^{11} pfu in 200 µl (Final

Concentration: $1x10^{11}$ pfu/ml; Ca/P: 5.28/3.16 mM) in a 96-well plate. After that, 96-well plate was shaken at 150 rpm for 8 hours at 25°C. Mineral formation kinetics of each peptides were monitored once an hour using a UV Spectrophotometer by continuous measuring of absorbance at 820 nm for 10 seconds per minute (7 readings in total).

2.7. Fourier Transform Infrared Spectroscopy (FTIR) Analysis

For FT-IR analysis, mineralization reactions were set up for peptides initiated with 10^{11} pfu in 500 µl (Final Concentration: $1x10^{11}$ pfu/ml; Ca/P: 5.28/3.16 mM) in pre-sterilized 2 ml centrifuge tubes. In order to generate adequate mineral for the analysis, each reaction was performed four times with a total reaction volume of 2 mL. Following the reaction, samples were collected by centrifugation at 14K for 10 minutes and allowed to freeze-dry using Labconco Freezone 18 L Console for 24 hours. FT-IR analysis was performed using a PerkinElmer UATR Two-FT-IR Spectrometer. The frequency range was computed between 4000-400 cm^{-1} and spectra were collected at 1 cm^{-1} resolution over 20 scans.

2.8. X-Ray Diffraction (XRD) Characterization

Mineralization reactions for XRD characterization were performed precisely the same as for FTIR analysis having a total reaction volume of 3.5 mL to create sufficient mineral for the analysis. Following the reaction, samples were centrifuged at 14K for 10 minutes before being freeze-dried for 24 hours using the Labconco Freezone 18 L Console. The X-ray diffraction (XRD; Philips X'Pert Pro) examination provided detailed information about the material's crystallographic structure, chemical composition and physical properties. XRD patterns were obtained at 25°C in the range of 10 to 80˚ 2Ɵ with a resolution of 0.1˚; the resulting patterns were compared to International Centre for Diffraction Data (ICDD, formerly JCPDS) data.

CHAPTER 3

RESULTS & DISCUSSION

3.1. Effect of Ion Concentration on Homogenous Ca/P Mineralization

The objective in optimizing the effect of ion concentration was to achieve mineralization via peptides, while no mineralization occurred under predetermined pH, temperature and ion concentration conditions (Deniz T. Yucesoy et al. 2020, 2022, 2023). Hepes buffer was identified as the optimal buffering agent for the selective pressure optimization due its minor change in pKa with temperature proporties, temperature was set to 25°C and the reactants' pH were adjusted to 7.0 at 25°C. Therefore, the effect of ion concentration on Ca/P mineralization was utilized using 19.2 mM $CaCl_2.2H_2O$ (pH: 7.0 25°C), 11.52 mM KH_2PO_4 (pH: 7.0 25°C) and 50 mM HEPES (pH: 7.0 25°C). The reactions were carried out in seven setups: (i)100 µL Ca^{+2}, 100 µL PO_4^{-3} (Ca/P: 9.6/5.76 mM; 2x); (ii) 75 µL Ca^{+2}, 75 µL PO_4^{-3}, 50 µL Hepes (Ca/P:7.2/4.32 mM; 1.5x); (iii) 66 µL Ca^{+2}, 66 µL PO_4^{-3}, 66 µL Hepes (Ca/P: 6.38/3.83 mM; 1.33x); (iv) 50 µL Ca^{+2}, 50 µL PO_4^{-3}, 100 µL Hepes (Ca/P: 4.8/2.88 Mm; 1x); (v) 37,5 µL Ca^{+2}, 37,5 µL PO_4^{-3}, 125 µL Hepes (Ca/P: 3.6/2.16 mM), (vi) 33 µL Ca^{+2}, 33 µL PO_4^{-3}, 132 µL Hepes (Ca/P: 3.16/1.9 mM) and (vii) 25 µL Ca^{+2}, 25 µL PO_4^{-3}, 150 µL Hepes (Ca/P: 2.4/1.44 mM). The mineralization kinetics was measured at 820 nm during 10 seconds per 2 hours with low-continious shaking by UV-Vis Spectrophotometer. After 2 hours, absorbance increased from 0 to 0.05 for 1.33x, 0 to 0.08 for 1.5x and 0 to 0.1 for 2x; whereas an increase was absent at 1x, 0.75x, 0.66x and 0.5x (the Ca/P ratio of 4.8/2.88 mM was mentioned as 1x; 1.33x referred to the multiplied of Ca/P: 4.8/2.88 mM with 1.33, e.g., Ca/P: 6.38/3.83 mM; 0.75x referred to the multiplied of Ca/P: 4.8/2.88 mM with 0.75, e.g., Ca/P: 3.6/2.16 mM) (Figure 3.1.). This proved that, there was no mineralization while Ca/P $\leq$ 4.8/2.88 mM. Following a comprehensive evaluation, Hepes buffer was identified as the optimal buffering agent with a reaction temperature at 25°C, Ca/P concentration of 4.8/2.88 mM and a pH 7.0.

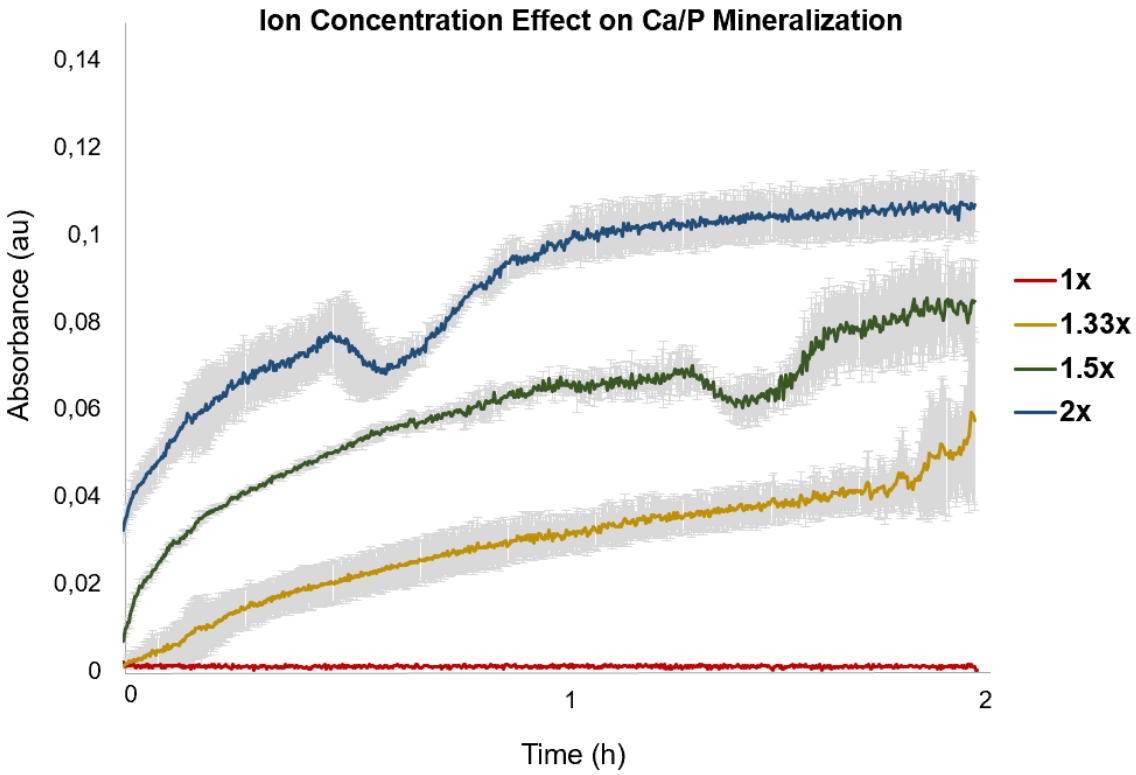

Figure 3.1. Effect of Ion Concentration on Ca/P Mineralization.

3.2. Selection of Mineralizing Peptides via Directed Evolution

Catalytic peptides with mineral formation fucntion were selected utilizing a directed evolution method through M13 Phage Display Library under predetermined selective pressure conditions (Zin et al. 2005; Smith and Petrenko 1997; Rath et al., n.d.; Whaley et al. 2000). In order to enrich the pool in favor of mineralizing peptide sequences, protocol was executed over four successive rounds of Biopanning (Figure 3.2.). The library cloning vector, M13KE stands out from the wild-type filamentous phage vector where the lacZα-peptide cloning sequence (assists in blue/white screening) has been inserted in the region of the (+) strand origin of replication, leading to a longer replication cycle (Noren and Noren 2000). Furthermore, displaying foreign peptides as N-terminal fusions to pIII (mediates infectivity by binding to the recipient bacterium's F-pilus) may reduce the phage's infectivity as contrasted with wild-type M13. These bring the possibility of any contaminating wild-type phage during the amplification steps between rounds of panning; even small levels of contamination can result in a majority of the phage pool being wild-type phage. In order to proceed in a controlled manner with

the selection process, the identified libraries, e.g., BP1-S1, BP1-M1, and BP1-M2, were plated on LB Agar-IPTG-Xgal plates before beginning the following biopanning round. Since the library cloning vector, M13KE, is derived from the cloning vector of M13mp19 which carries the lacZα gene whereas ER2738 lacks the lacZα gene; only the cells infected by M13mp19 bacteriophage can hydrolyze X-Gal and form blue phage plaques (Ullmann A, Jacob F, and Monod J 1967; Van Wezenbeek PM, Hulsebos TJ, and Schoenmakers JG 1980). Blue-White Colony screening also enabled us to determine the concentration of the phages, which was computed using Eq. 2.1. Figure 3.3. presents the depiction of the methodology for determining the concentration of BP1-M2 through blue-white colony screening. As deliniated in Eq. 2.1., the calculation of the phage titer expressed in plaque forming units (pfu) per 1000 µl (ml); necessitates the multiplication of the number of blue plaques by the dilution factor, volume and µl conversion (Baer and Kehn-Hall 2014). The quantification process at a dilution level of 10^10 revealed that the quantity of blue plaques exceeded the capacity for accurate enumeration. Hence, the quantification was undertaken at 10^11, and eight blue colonies were counted. The number of counts was then multiplied by the dilution factor, 10^11. Given that a sample volume of 20 microliters was used for LB Agar plating, we multiplied by 20. Additionally, because the initial stock volume of BP1-M2 was 200 microliters, a conversion factor of 5 was used to standardize the volume to 1000 microliter. Table 3.1. indicated the phage concentrations quantified by Blue-White Colony Screening.

The concentration of purified phages from each biopanning round was also measured by Nanodrop 8000 with a wavelenght range of 269-320 nm and calculated through the equation given in Eq. 2.2. The UV absorption spectrum of phage purified by PEG-precipitation and dissolved in TBS exhibited a shallow maximum around 269 nm. M13KE has 7200 base-pairs, hence the concentration (pfu/ml) was calculated by multiplying the difference in absorbance at 269 and 320 nm by 6x10^6 and dividing by 7200 (Noren and Noren 2000). Since plating and nanodrop measurements were consistent, each biopanning round were started based on plating concentrations.

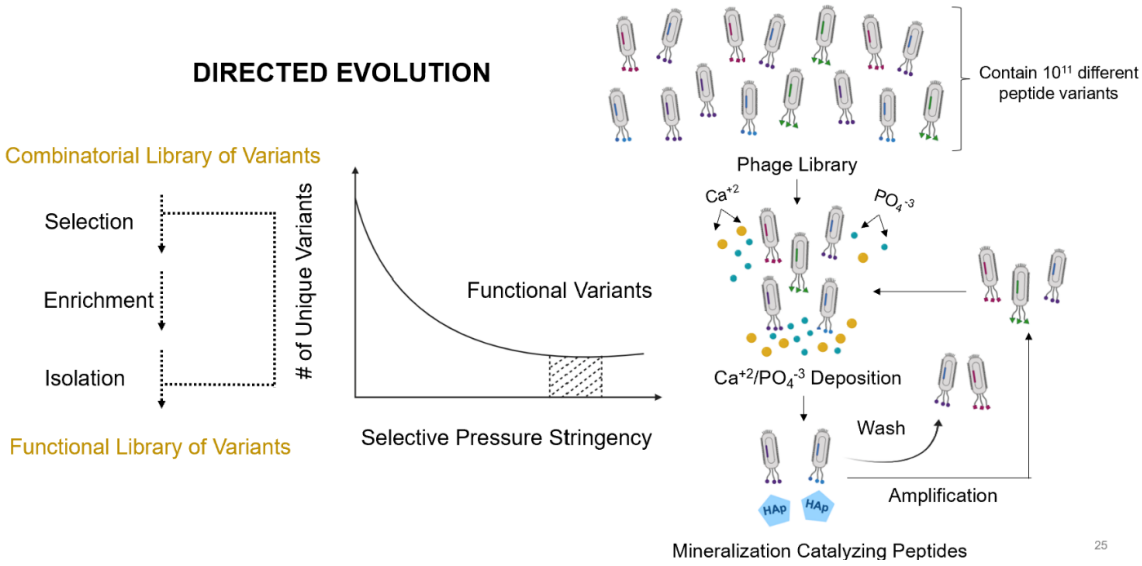

Figure 3.2. Selection of Mineralizing Peptides via Directed Evolution.

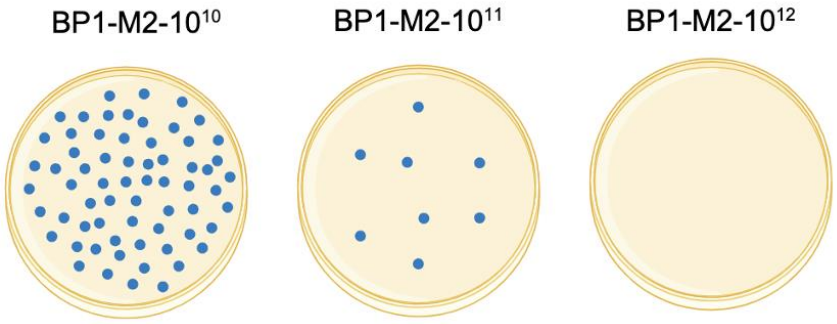

Figure 3.3. Depiction of the Methodology for Determining the Concentration of BP1-M2.

Table 3.1. Quantification of Phages via Blue-White Colony Screening;

Biopanning Rounds	**Concentration (pfu/ml)**
BP1-S1 (no detergent)	$<1x10^7$
BP1-M1	$1{,}01x10^9$
BP1-M2	$1x10^{13}$
BP2-S1 (no detergent)	$<1x10^7$
BP2-S2 (%0.01 detergent)	$<1x10^7$
BP2-S3 (%0.01 detergent)	$<1x10^7$

(Cont. on next page)

Table 3.1. (Cont.)

BP2-M1	$1{,}21 \times 10^{10}$
BP2-M2	$3{,}40 \times 10^{13}$
BP3-S1 (no detergent)	1.7×10^{8}
BP3-S2 (%0.01 detergent)	1×10^{9}
BP3-S3 (%0.02 detergent)	1×10^{9}
BP3-M1	$2{,}12 \times 10^{10}$
BP3-M2	1×10^{13}
BP4-S1 (no detergent)	1×10^{9}
BP4-S2 (%0.01 detergent)	1×10^{9}
BP4-S3 (%0.05 detergent)	1×10^{9}
BP4-M1	$2{,}39 \times 10^{10}$
BP4-M2	5×10^{13}

Mineral formation capability of the enrichment peptide library from each biopanning round were monitored using a UV Spectrophotometer by continuous measuring of absorbance at 820 nm during 24 hours. As seen in Figure 3.4., Ca/P mineralization was observed through presence of enrichment peptide libraries, whereas no mineralization was observed in the absence of the peptide. These results proved the success of the enrichment.

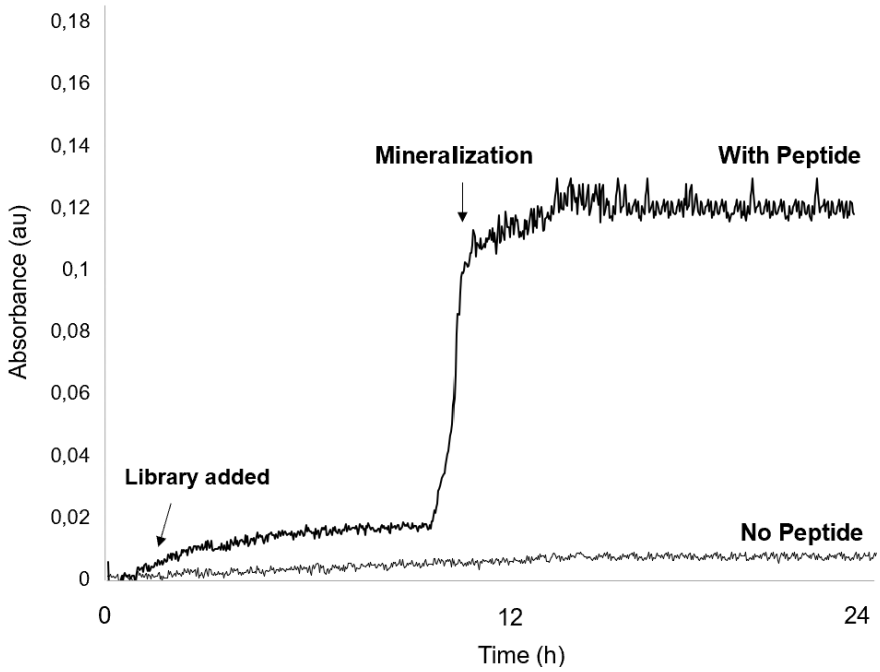

Figure 3.4. Ca/P Mineralization Analysis via Peptide Library.

3.3. Selection of Peptides from Biopanning Round IV

BP4-M2 enrichment library was serial diluted into 10^9 pfu that resulted ~80-100 peptides on LB Agar-IPTG-Xgal plate. 80 peptides were picked up by pipettor tip; put seperately into 150 µl of PC Buffer in pre-sterilized 1.5 ml DNAse free centrifuge tubes (Figure 3.5.). These tubes were shaken for 15 min at 150 rpm and incubated 60°C for 45 minutes and kept at 4°C for O/N. Next day, 150 µl of phage solution was transferred into 150 µl glycerol stocks (%50 glycerol) and was stored at -20°C.

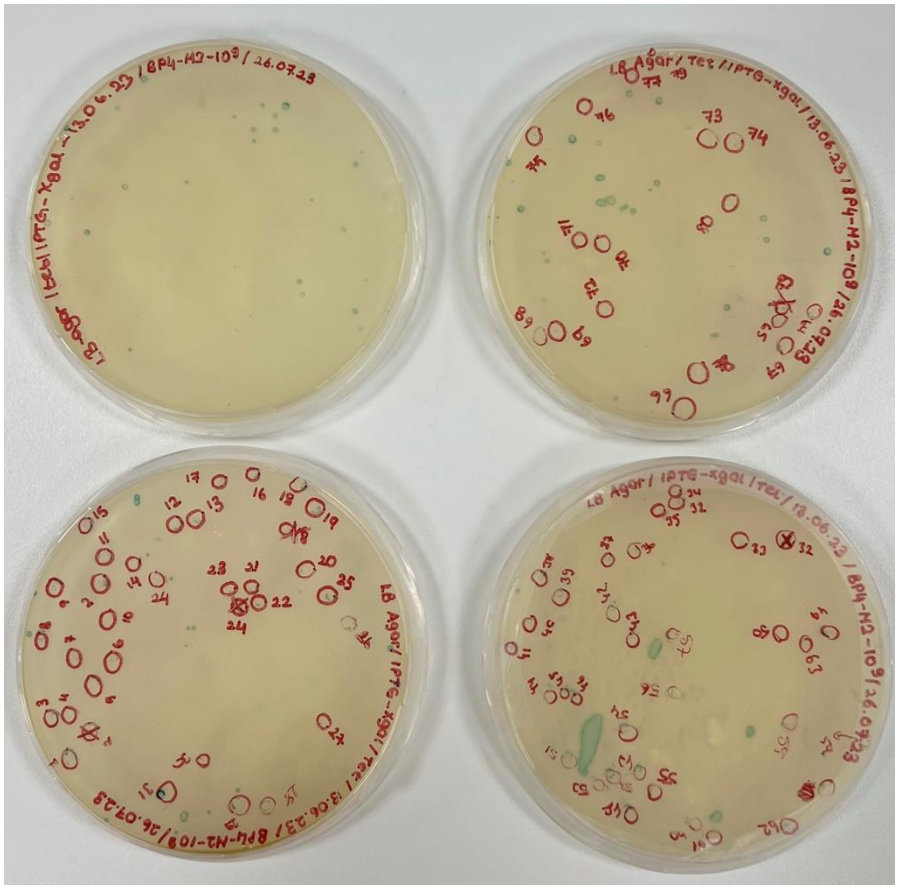

Figure 3.5. Selection of Peptides from BP4-M2; 80 colonies were selected.

3.4. ssDNA Isolation & Sequencing

16 ssDNAs from Biopanning Round IV-Selected Peptides were isolated using the QIAprep Spin M13 Kit. The isolated DNAs were quantified via Nanodrop 8000 at 600 nm. The absorbance ratio of 260/280 nm was used to evaluate DNA purity; a ratio of ~1.8 was considered as "pure" for DNA. A ratio of ≤ 1.6 indicated the presence of proteins, phenol or other contaminants that absorb at 280 nm; whereas if the ratio ≥ 1.8, indicated the presence of RNA contamination (Lucena-Aguilar et al. 2016). Meanwhile, the 260/230 ratio was utilized to indicate the presence of undesirable chemical compounds including Trizol, phenol or Guanidine HCl. The expected range for 260/230 values were in 2.0-2.2; a ratio below than expected, indicated the presence of Ethanol or EDTA contaminant which absorb at 230 nm (Usman et al. 2014; HASSAN MMed et al. 2015). As illustrated in Table 3.2., the isolated DNAs purities and concentrations (should ≥ 20 ng/µl) of the peptides were appropriate for the sequencing. Sanger sequencing was

performed on 16 peptides. For sequence analysis tool, "Just Bio" was utilized to obtain complementary of the DNA sequence and to translate DNA sequences from 1 to 6 phases yielding formated outputs. Furthermore, protparam tool was used for computing physical (molecular weight, charge) and chemical parameters (theoretical pI, average of hydropathicity, GRAVY) for a given aminoacid sequence (Table 3.3.).

Table 3.2. DNA Concentration and Purity;

Peptide ID	260/280	260/230	Concentration (ng/µl)
MP22	2,14	3,77	20,9
MP23	1,84	1,39	36,72
MP24	1,95	1,87	38,22
MP25	1,96	1,59	33,1
MP26	1,91	2,02	37,05
MP27	1,43	0,15	24,28
MP28	1,86	1,93	38
MP29	1,96	1,29	57,88
MP30	2,05	2,04	84,08
MP31	1,85	2,27	52,81
MP32	2,11	1,83	41,67
MP33	1,92	1,98	34,12
MP34	2,04	2,98	27,93
MP35	1,79	2,47	33,29
MP36	1,85	2,83	36,29
MP37	1,91	2,59	38,8

Table 3.3. Physical and Chemical Parameters of Peptides;

Peptide ID	MW	pI	G.R.A.V.Y.	Charge
MP22	1129.30	6.74	0.767	0
MP23	1223.25	8.46	0.308	+1
MP24	1221.38	8.31	-0.736	+1
MP26	1368.57	8.50	-1.042	+1

(Cont. on next page)

Table 3.3. Cont.

MP27	1227.33	3.80	0.692	-1
MP28	1315.45	8.33	-1.033	+1
MP30	1220.35	8.76	-0.808	+1
MP31	1334.77	10.00	-2.067	+2
MP32	1432.67	5.08	-0.217	-1
MP34	1292.46	9.76	-0.173	+1
MP35	1380.53	5.52	-0.225	0
MP36	1224.11	8.59	0.027	+1
MP37	1298.49	3.56	0.692	-2

3.5. Peptide Amplification & Purification & Quantification

Upon Sanger Sequencing examination, nine out of the 16 peptides were observed to be devoid of aminoacid sequences. Each of the peptides selected in Section 3.4. with known sequences has been amplified and purified (7 in total), in order to increase the number of copies for their kinetic and structural investigations. The concentration of amplified & purified peptides was quantified by Nanodrop 8000 with a wavelenght range of 269-320 nm and calculated through the equation given in Eq. 2.2. The UV absorption spectrum of the peptide purified by PEG-precipitation and dissolved in TBS exhibited a shallow maximum around 269 nm. M13KE has 7200 base-pairs, hence the concentration (pfu/ml) was calculated by multiplying the difference in absorbance at 269 and 320 nm by $6x10^6$ and dividing by 7200 (Noren and Noren 2000). Table 3.4. indicated the purified peptide concentrations quantified by Nanodrop.

Table 3.4. Quantification of the Peptides;

Peptide ID	Concentration (pfu/ml)
MP22	$2,83x10^{12}$
MP23	$6,69x10^{12}$
MP24	$3,72x10^{12}$

(Cont. on next page)

Table 3.4. Cont.

MP26	$8,79x10^{12}$
MP27	$6,75x10^{12}$
MP28	$2,74x10^{12}$
MP30	$2,50x10^{12}$

3.6. Mineralization Kinetic Analysis with Peptides

Mineralization reactions for each peptide were commenced with 10^{11} pfu in 200 µl (Final Concentration: $1x10^{11}$ pfu/ml; Ca/P: 5.28/3.16 mM). The mineral formation kinetics of each peptide were monitored once an hour for 7 hours by continuously measuring absorbance at 820 nm. As shown in Figure 3.6., Mineralizing Peptide 23 (MP23) and Mineralizing Peptide 22 (MP22) exhibited the fastest mineral formation rates reaching 0.08 at the fourth hour; whereas the absorbance of the negative control reached to 0.02 and remained constant in subsequent hours. This observation proved that the peptides not only facilitated rapid minerals but also exceeded the mineral production of the negative control. Conversely, MP30 exhibited slower mineralization kinetics, achieving an absorbance of 0.01 after 6 hours. The reaction kinetics was further quantified by monitoring the rate of Ca^{2+} consumption at different time points by ICP-OES. The results of the kinetic measurements revealed that the Ca^{2+} consumption rate of peptides over 4 hours were 0.125 ng/min, 0.06 ng/min and 0.018 for MP23, MP22 and MP30 respectively (Figure 3.7.).

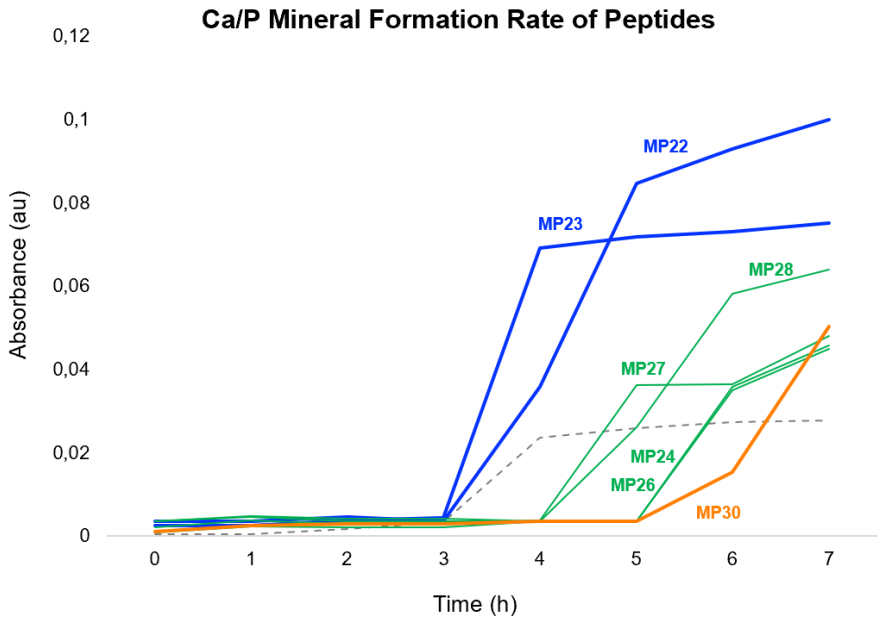

Figure 3.6. Mineral Formation Rate of Peptides.

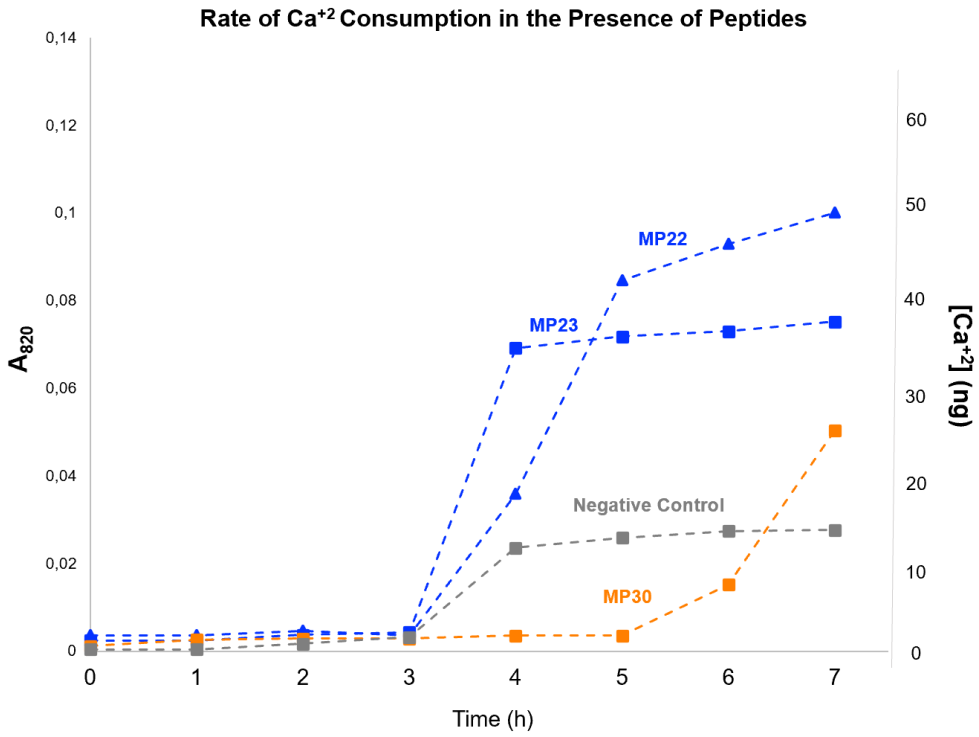

Figure 3.7. Rate of Ca^{2+} Consumption in the Presence of Peptides.

3.7. Fourier Transform Infrared Spectroscopy (FTIR) Analysis

The structural analysis and quantification of the crystallinity indexes of the minerals produced in the presence of the mineralization catalyzing peptides was observed by FTIR Spectrophotometry and the frequency range was computed in 4000-400 cm^{-1} (Appendix B). Structural analysis of the minerals were compared against the infrared spectra of the merck hydroxyapatite (HAp) powder. Hydroxyapatite mineral consists of phosphate, carbonate and hydroxyl groups which make it active in the vibrational range of the infrared spectrum. For example, the peaks recognized at 1086 and 1025 cm^{-1} indicated the asymmetric stretching vibration (v3) of the phosphate group and the peak at 962 cm^{-1} corresponds to the symmetric stretching vibration (v1). Furthermore, it has bending vibrations on the v4 state between 567-601 cm^{-1} and v2 bending vibration at 962 cm^{-1}. Last but not least, the presence of hydroxyl groups are observed at 630 and 3550 cm^{-1}; likewise, the carbonate group's asymmetric stretching vibration (v3) is observed at 1456-1417 cm^{-1}. FTIR spectra of characterized HAp have been found to correlate with the literature (Rehm and Bonfield 1997; Sahadat Hossain and Ahmed 2023; Nguyen et al. 2013; Suffo-Pino et al. 2023). As illustrated in Figure 3.8, compared to negative controls, the minerals catalyzed by the peptides exhibited comparable peaks within the HAp, thereby confirmed the formation of hydroxyapatite in the presence of the peptides. While there was an absence of peaks in the negative control in the 1456-1417 cm-1 range, these peaks appared in the presence of the peptides, which may indicate their involvement in carbonylation. Moreover, MP23 exhibited citrate addition at 2980 cm^{-1} while no peak exhibited with MP22 and MP30. This could imply inter-peptide differences. 2980 cm^{-1} may be related to the -CH2 band of OCP-Citrate, which is in the octacalcium phosphate (OCP) dicarboxylate group. Octacalcium phosphate carboxylates has structural similarities within the parent compound OCP and the general formula of OCP-Citrate is $Ca_8(HPO_4)_{1.60}(cit)_{0.40}(PO_4)_4 7.8H_20$ (Markovic and Brownla 1993; B. 0 Fowler, Moreno, and Brown 1966). Mineral crystallinity was also evaluated with the data obtained from FTIR. Crystallinity index was calculated from FTIR peaks by dividing the sum of the peaks representing O–P–O bending of phosphate in HAp (between 567 cm1 and 601 cm-1) by the height of the valleys between them (Figure 3.9.) (Weiner' and Bar-Yosefa 1990; Choi et al. 2015). Figure 3.10 illustrated the crystallinity index values of the peptides ranging between 2.40-2.60 compared with the standard HAp whose crystallanity index

value is 5 (Shlaferman et al. 2019; Baillargeon et al. 2017). As a conclusion, structural analysis and quantification of the crystallinity indexes revealed that the peptides have an ability to generate hydroxyapatite with a sufficient crystal index. In accordance of these results, a novel investigation was emerged to investigate the ability of these peptides to induce HAp formation apart from HAp stoichiometry. MP23, chosen for this investigation due to its fast mineral formation ability, was characterized under tricalcium-phosphate (TCP) stoichiometric conditions with a Ca/P ratio of 1.5. (Gungormus et al. 2012a). Within the experimental framework, the calcium ratios were held constant and the amount of phosphate changed for the attainment of the desired ratio. Mineralization reactions were initiated with 10^{11} pfu in 500 µl (Final Concentration: $1x10^{11}$ pfu/ml; HAp → Ca/P: 5.28/3.16 mM; TCP –> Ca/P: 5.28/3.51 mM) in pre-sterilized 2 ml centrifuge tubes and the frequency range was computed between 4000-400 cm^{-1}. The FTIR spectrum of merck TCP have revealed similar characteristic peaks to those of HAp; nevertheless, within the spectrum range of 1400-1460 cm-1, distinctive bands unique only to HAp, were discerned which was related with the asymmetric stretching vibration of its carbonate group; while this peak was observed in HAp at 1456 and 1417 cm-1, but not in TCP (Figure 3.11.). Therefore, the primary question was whether the peak at 1456 and 1417 cm-1 would be observed under MP23 in TCP stoichiometric conditions. As illustrated in Figure 3.12, while no detectable peak was observed in 1456-1417 cm^{-1} both positive and negative controls within the HAp stoichiometry; MP23 exhibited a conspicuous peak within the intended 1456-1417 cm^{-1} range. Furthermore, while the absence of the peak was observed attributed to the -CH2 band at negative control, it was observed in the presence of the peptide. These observations suggested the potential of MP23 in the formation of carbonate and citrate adduction in HAp stoichiometry. Furthermore, in Figure 3.13, an absence of peaks within the 1456-1417 cm-1 range was evident in both positive and negative controls under TCP stoichiometric conditions; conversely MP23 exhibited a prominent peak within this specified range. Additionally, while the presence of the peak was observed attributed to the citrate addition at negative control was not observed in the presence of the peptide. These observations indicate the potential of MP23 have a role only in carbonate formation under TCP stoichiometry, in contrast to its behavior in HAp stoichiometry. As a result, MP23 had proved to govern HAp mineralization apart from the HAp stoichiometry.

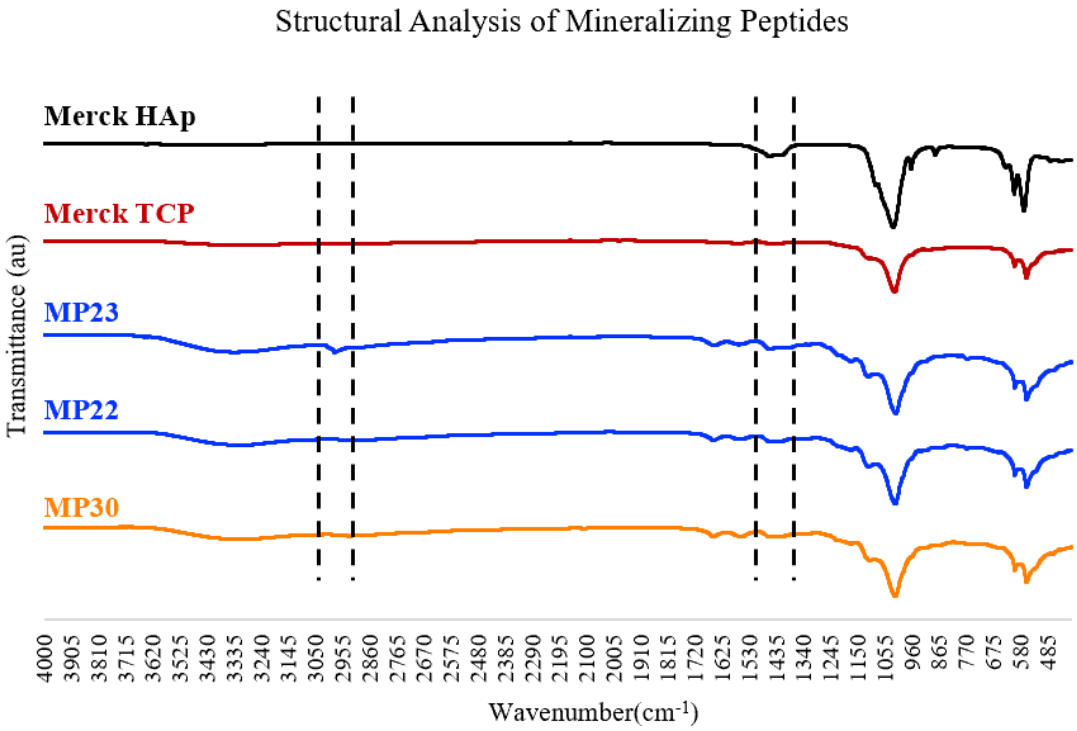

Figure 3.8. Structurcal Analysis of Mineralizing Peptides.

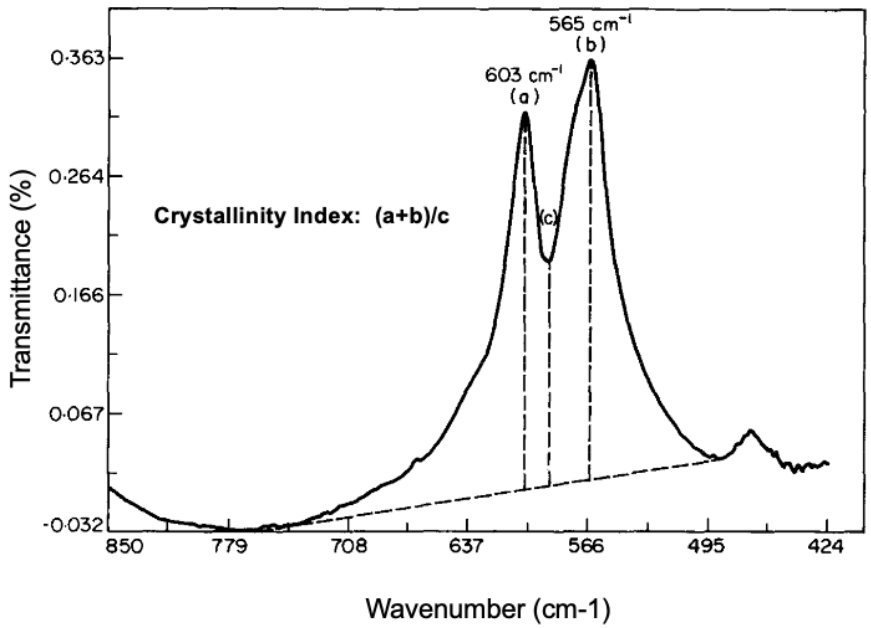

Figure 3.9. Calculation of Crystallinity Index.

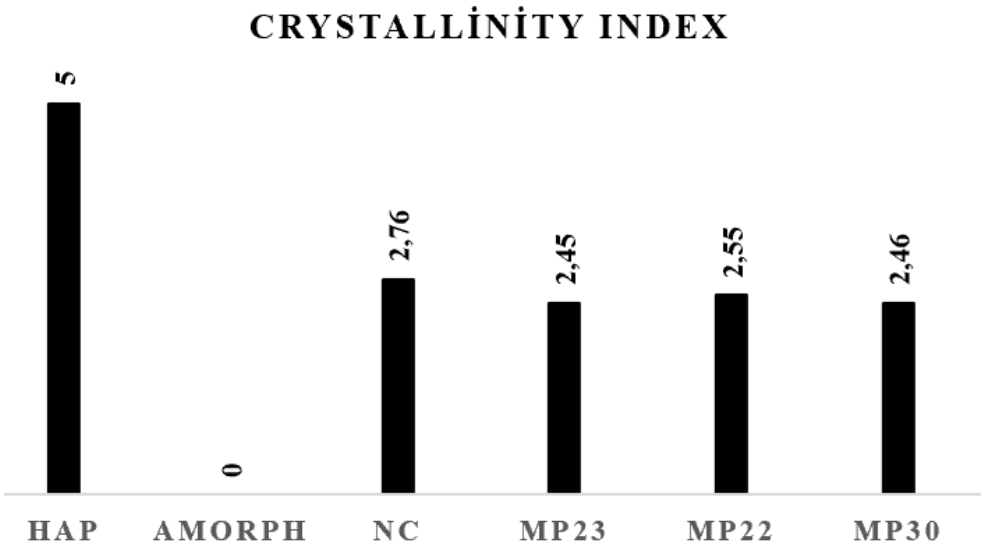

Figure 3.10. Crystallinity Index (CI) Values of Minerals Catalyzed by Peptide.

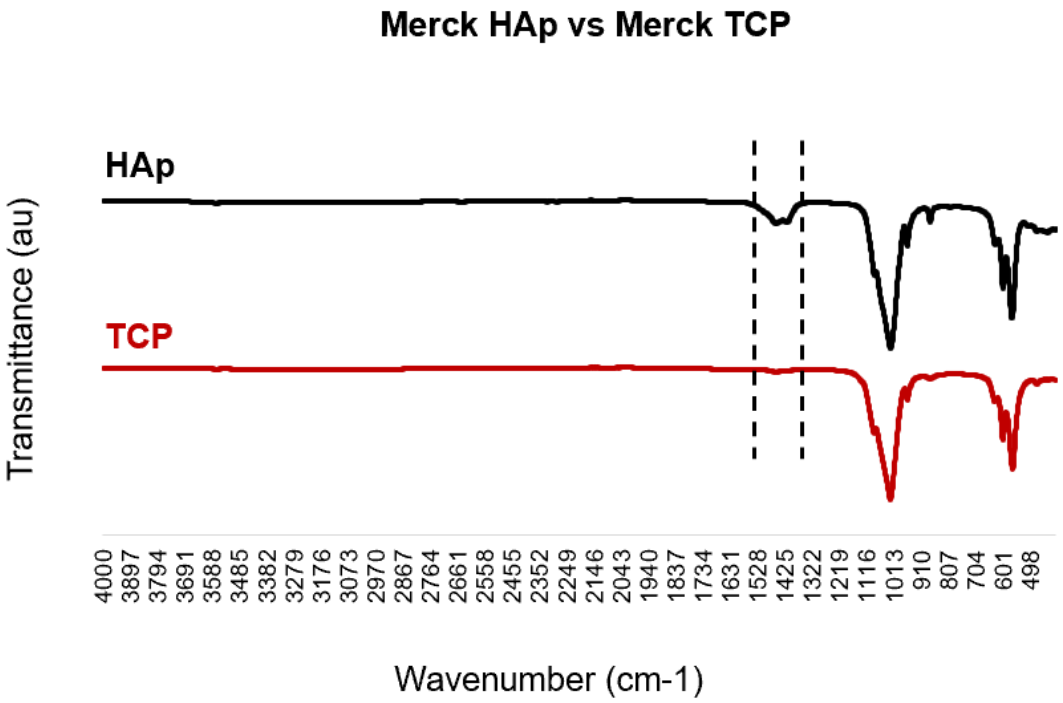

Figure 3.11. IR Spectrum of Merck HAp vs Merck TCP.

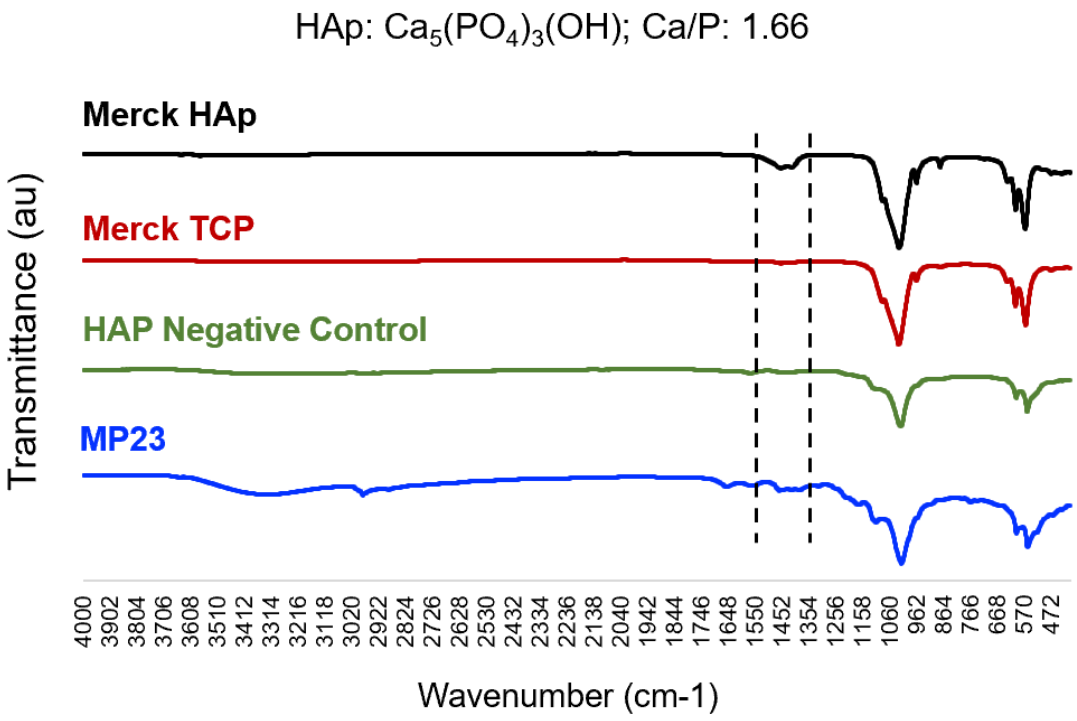

Figure 3.12. Structural Analysis of MP23 in HAp Stoichiometry.

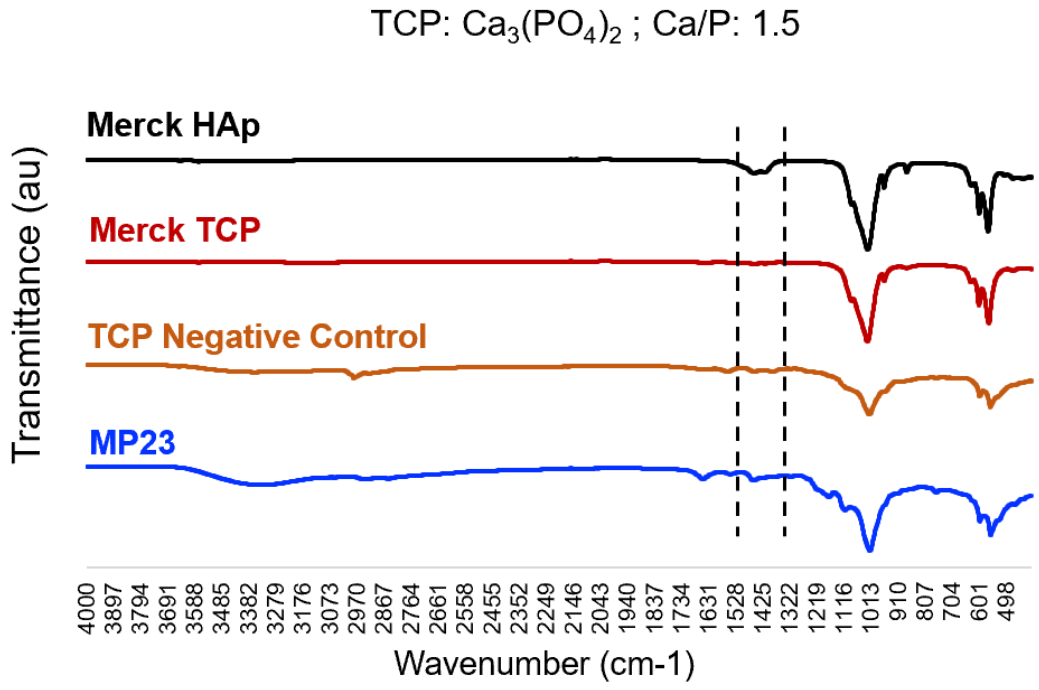

Figure 3.13. Structual Analysis of MP23 in TCP Stoichiometry.

3.8. X-Ray Diffraction (XRD) Analysis Characterization

The crystallographic analysis via XRD confirmed that, the mineral formed by MP23 displayed the numerous sharp peaks indicative of characteristic peaks belonging to the crystalline HAp while the mineral formed by negative conrol displayed weaker diffraction peaks (Figure 3.14.) (Phatai et al. 2018). This result indicated that the hydroxyapatite mineral formed by MP23 exhibited significantly higher crystallinity compared to the mineral formed in the negative control.

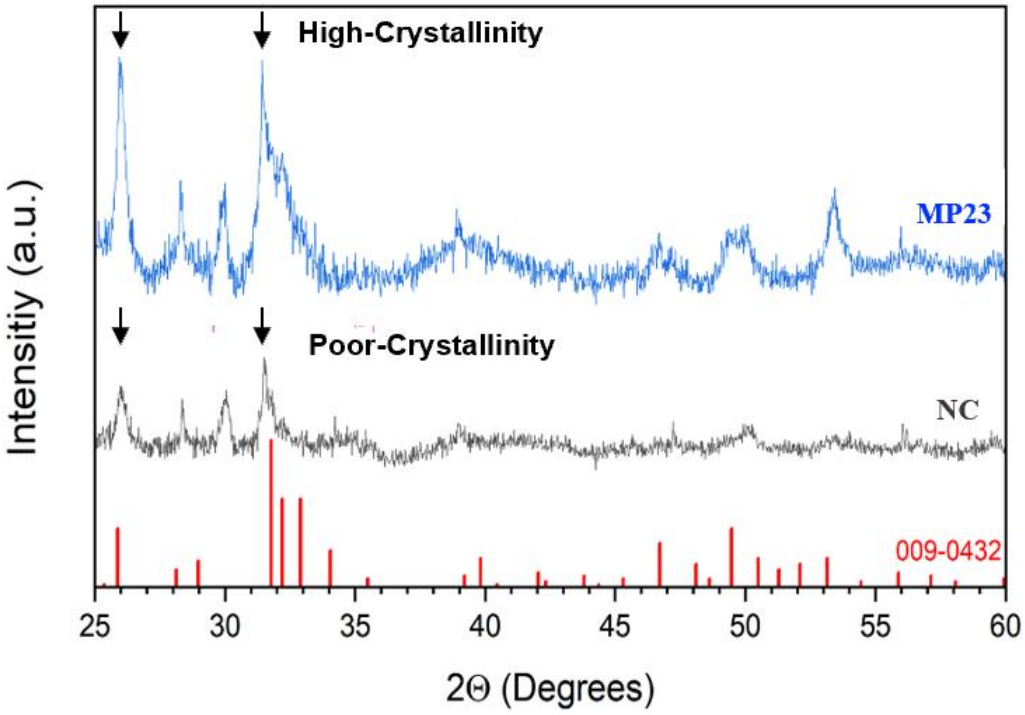

Figure 3.14. XRD patterns of the minerals formed by MP23 and Negative Control Compared to ICDD HAp (JCPDS 09-0432).

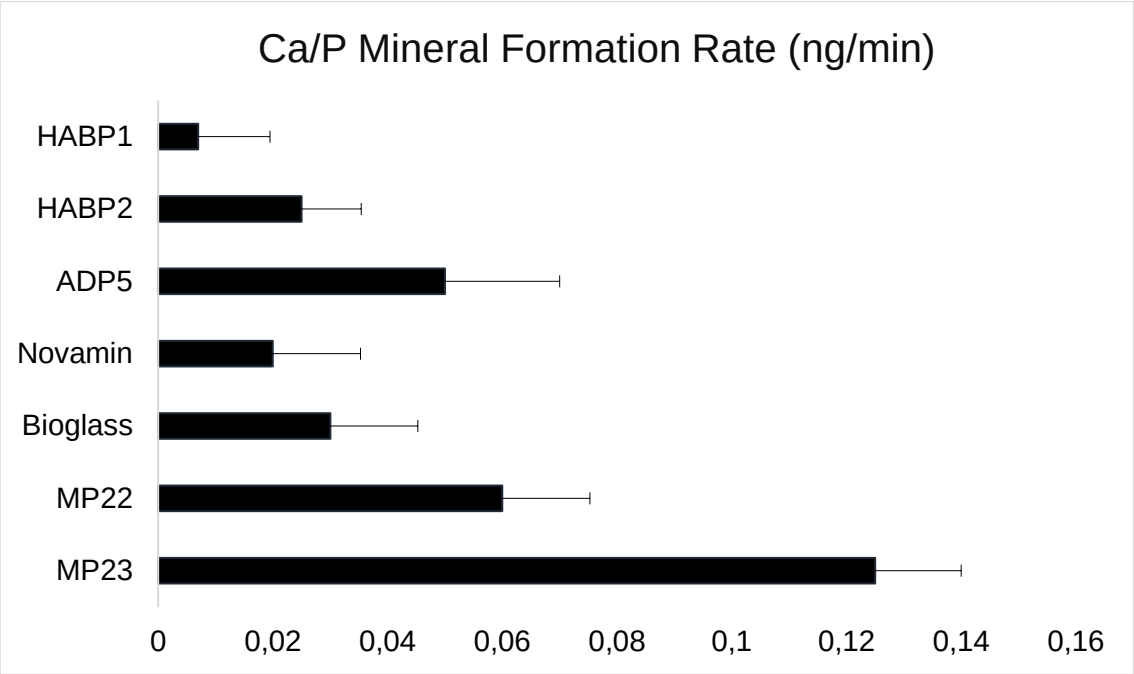

Figure 3.15. Comparative Analysis of Mineral Formation Rate of Peptides with State of Arts.

CHAPTER 4

CONCLUSION

Inspired by biology at the nanoscale, the aim of this thesis was to identify novel methodology to identify short catalytic peptides that can govern hydroxyapatite (HAp) mineralization and exhibit fast mineral formation rate in an aqueous media similar to natural proteins with directed evolution approach. The criterion success of identifying peptides with inherent catalytic capabilities that directly induce mineralization was facilitating mineral formation rate faster than the state of art. For that purpose, first of all, selective pressure parameters (reactants' pH, reaction temperature, buffer type and ion concentrations) were optimized for identifying mineralizing peptides. Following a comprehensive evaluation, Hepes buffer was identified as the optimal buffering agent with a reaction temperature at 25°C, Ca/P concentration of 4.8/2.88 mM and the pH of 7.0. Subsequently, mineralization catalyzing peptides were selected throughout four biopanning rounds to enrich the pool in favor of mineralizing catalytic sequences utilizing a directed evolution method through M13 Phage Display Library. The selection proved the success of the enriched peptide libraries promoting Ca/P mineralization, whereas no mineralization was observed in the absence of the peptide. Following within the obtained success criterion, 80 peptides were selected from Biopanning Round IV, with 37 of these peptides exhibited different sequences. 31 of these peptides exhibiting different sequences were amplified & purified and subjected to further analyses through kinetic measurements and structural characterizations. Although enrichment peptide libraries carry out mineralization at a Ca/P: 4.8/2.88 ratio; mineralization was observed at the end of the 24th hour, indicating the limited effectiveness of peptides under biological conditions. Consequently, the ion concentration was increased slightly over the critical level and the kinetic rates of the peptides selected from Biopanning Round IV were investigated at a Ca/P ratio of 5.28/3.16 mM. Mineral formation rates of the peptides were monitored by continious measuring of absorbance at 820 nm wavelenght using a UV-Spectrophotometer. MP23 exhibited the fastest mineral formation rates reaching 0.08 at the fourth hour; whereas the absorbance of the negative control reached to 0.02 and remained constant in subsequent hours. This observation proved that the peptides not only facilitated rapid minerals but also exceeded the mineral production of the negative

control. Conversely, MP30 exhibited slower mineralization kinetics, achieving an absorbance of 0.01 after 6 hours. The reaction kinetics was further quantified by monitoring the rate of Ca^{2+} consumption by ICP-OES. Ca^{2+} consumption rate of peptides over 4 hours obeyed their absorbance reaction kinetics with constans of 0.125 ng/min, 0.06 ng/min and 0.018 ng/min for MP23, MP22 and MP30 respectively. Kinetic measurements revealed that MP23 catalyze Ca/P mineralization four times faster than Bioglass & Novamin, 16 times faster than HABP1, 5 times faster than HABP2 and 5 times faster than ADP5 (Figure 3.15.). Structural analysis by FTIR and quantification of the crystallinity indexes revealed that the peptides have an ability to generate hydroxyapatite mineral with a sufficient crystal index (2.40-2.60). MP23 exhibited citrate addition at 2980 cm^{-1}, whereas MP22 and MP30 did not demonstrate this characteristic peak; which could imply inter-peptide differences. Furthermore, MP23 proved to govern HAp mineralization apart from the HAp stoichiometry. Last but not least, XRD analysis confirmed the formation of hydroxyapatite mineral in the presence of MP23 exhibited high-crystallinity; whereas the negative control displayed poor crystallinity. As a brief, it was developed a novel methodology to identify peptides with mineralization functions, surpassing traditional approaches based on binding activity or protein domains/fragments (Fan, Sun, and Moradian-Oldak 2009a; Gungormus et al. 2008). Within this methodology, it was identified a set of peptides notably one that accelerates the kinetics of calcium/phosphate reaction ∼15 times faster than existent state-of-the-art peptides (Gungormus et al. 2008, 2012b; Dogan et al. 2018a). The structural and morphological analyses was further highlighted these peptides' potential in biomineralization. These identified peptide sequences could serve as foundational elements in the development of clinical products as dental gels and toothpaste formulations. Furthermore, these findings would be a strong potential for restoring demineralized tissues and treating diseases related to pathological biomineralization.

REFERENCES

Abelson, D C, and I D Mandel. 1981. “The Effect of Saliva on Plaque PH in Vivo.” *J Dent Res*. Vol. 60.

Addadi, Lia, and Steve Weiner. 2014. “Biomineralization: Mineral Formation by Organisms.” *Physica Scripta* 89 (9). doi:10.1088/0031-8949/89/9/098003.

An, G. H., H. J. Wang, B. H. Kim, Y. G. Jeong, and Y. H. Choa. 2007. “Fabrication and Characterization of a Hydroxyapatite Nanopowder by Ultrasonic Spray Pyrolysis with Salt-Assisted Decomposition.” *Materials Science and Engineering: A* 449–451 (March). Elsevier BV: 821–24. doi:10.1016/j.msea.2006.02.436.

Arshad, Saba, Syed Jaffar Abbas Zaidi, and Waqas Ahmed Farooqui. 2021. “Comparative Efficacy of BioMin-F, Colgate Sensitive Pro-Relief and Sensodyne Rapid Action in Relieving Dentin Hypersensitivity: A Randomized Controlled Trial.” *BMC Oral Health* 21 (1). BioMed Central Ltd. doi:10.1186/s12903-021-01864-x.

Baelum, V., W. Van Palenstein Helderman, A. Hugoson, R. Yee, and O. Fejerskov. 2007. “A Global Perspective on Changes in the Burden of Caries and Periodontitis: Implications for Dentistry.” *Journal of Oral Rehabilitation* 34 (12): 872–906. doi:10.1111/j.1365-2842.2007.01799.x.

Baer, Alan, and Kylene Kehn-Hall. 2014. “Viral Concentration Determination through Plaque Assays: Using Traditional and Novel Overlay Systems.” *Journal of Visualized Experiments*, no. 93 (November). Journal of Visualized Experiments. doi:10.3791/52065.

Baillargeon, K. R., K. Meserve, S. Faulkner, S. Watson, H. Butts, P. Deighan, and A. E. Gerdon. 2017. “Precipitation SELEX: Identification of DNA Aptamers for Calcium Phosphate Materials Synthesis.” *Chemical Communications* 53 (6). Royal Society of Chemistry: 1092–95. doi:10.1039/c6cc08687j.

Beltrán-Aguilar, Eugenio D., Jonathan W. Goldstein, and Stuart A. Lockwood. 2000. “Fluoride Varnishes: A Review of Their Clinical Use, Cariostatic Mechanism, Efficacy and Safety.” *Journal of the American Dental Association* 131 (5). doi:10.14219/jada.archive.2000.0232.

Beniash, Elia, Cayla A. Stifler, Chang Yu Sun, Gang Seob Jung, Zhao Qin, Markus J. Buehler, and Pupa U.P.A. Gilbert. 2019. “The Hidden Structure of Human Enamel.” *Nature Communications* 10 (1). doi:10.1038/s41467-019-12185-7.

Bernardo, Mario, Henrique Luis, Michael D. Martin, Brian G. Leroux, Tessa Rue, Jorge Leitão, and Timothy A. Derouen. 2007. “Survival and Reasons for Failure of Amalgam versus Composite Posterior Restorations Placed in a Randomized Clinical Trial.” *Journal of the American Dental Association* 138 (6). American Dental Association: 775–83. doi:10.14219/jada.archive.2007.0265.

Bishara, Samir E., and Adam W. Ostby. 2008. “White Spot Lesions: Formation, Prevention, and Treatment.” *Seminars in Orthodontics* 14 (3): 174–82. doi:10.1053/j.sodo.2008.03.002.

Burwell, Anora K., Taili Thula-Mata, Laurie B. Gower, Stefan Habeliz, Michael Kurylo, Sunita P. Ho, Yung Ching Chien, et al. 2012. “Functional Remineralization of Dentin Lesions Using Polymer-Induced Liquid-Precursor Process.” *PLoS ONE* 7 (6). Public Library of Science. doi:10.1371/JOURNAL.PONE.0038852.

Buzalaf, Marília Afonso Rabelo, Angélicas Reis Hannas, and Melissa Thiemi Kato. 2012. “Saliva and Dental Erosion.” *Journal of Applied Oral Science*. doi:10.1590/S1678-77572012000500001.

Cai, Yurong, and Ruikang Tang. 2008. “Calcium Phosphate Nanoparticles in Biomineralization and Biomaterials.” *Journal of Materials Chemistry* 18 (32). Royal Society of Chemistry: 3775–87. doi:10.1039/b805407j.

Carvalho, Joana Christina, and Ulrich Schiffner. 2019. “Dental Caries in European Adults and Senior Citizens 1996-2016: ORCA Saturday Afternoon Symposium in Greifswald, Germany - Part II.” *Caries Research*. doi:10.1159/000492676.

Cheng, Ran, Hui Yang, Mei Ying Shao, Tao Hu, and Xue Dong Zhou. 2009. “Dental Erosion and Severe Tooth Decay Related to Soft Drinks: A Case Report and Literature Review.” *Journal of Zhejiang University: Science B* 10 (5): 395–99. doi:10.1631/jzus.B0820245.

Chien, Yung Ching, Jinhui Tao, Kuniko Saeki, Alexander F. Chin, Jolene L. Lau, Chun Long Chen, Ronald N. Zuckermann, Sally J. Marshall, Grayson W. Marshall, and James J. De Yoreo. 2017. “Using Biomimetic Polymers in Place of Noncollagenous Proteins to Achieve Functional Remineralization of Dentin

Tissues." *ACS Biomaterials Science and Engineering* 3 (12). American Chemical Society: 3469–79. doi:10.1021/acsbiomaterials.7b00378.

Cho, Jung Sang, and Yun Chan Kang. 2008. "Nano-Sized Hydroxyapatite Powders Prepared by Flame Spray Pyrolysis." *Journal of Alloys and Compounds* 464 (1–2): 282–87. doi:10.1016/j.jallcom.2007.09.092.

Choi, Siyoung, Scott Coonrod, Lara Estroff, and Claudia Fischbach. 2015. "Chemical and Physical Properties of Carbonated Hydroxyapatite Affect Breast Cancer Cell Behavior." *Acta Biomaterialia* 24 (September). Elsevier Ltd: 333–42. doi:10.1016/j.actbio.2015.06.001.

Dodds, M W J, S C Hsieh, and D A Johnson. 1991. "The Effect of Increased Mastication by Daily Gum-Chewing on Salivary Gland Output and Dental Plaque Acidogenicity." *J Dent Res*. Vol. 70.

Dogan, Sami, Hanson Fong, Deniz T. Yucesoy, Timothee Cousin, Carolyn Gresswell, Sefa Dag, Greg Huang, and Mehmet Sarikaya. 2018a. "Biomimetic Tooth Repair: Amelogenin-Derived Peptide Enables in Vitro Remineralization of Human Enamel." *ACS Biomaterials Science and Engineering* 4 (5). American Chemical Society: 1788–96. doi:10.1021/acsbiomaterials.7b00959.

Dorozhkin, Sergey V. 2011. "Calcium Orthophosphates: Occurrence, Properties, Biomineralization, Pathological Calcification and Biomimetic Applications." *Biomatter*. doi:10.4161/biom.18790.

Dorozhkin, Sergey V., and Matthias Epple. 2002. "Biological and Medical Significance of Calcium Phosphates." *Angewandte Chemie - International Edition*. doi:10.1002/1521-3773(20020902)41:17<3130::AID-ANIE3130>3.0.CO;2-1.

Dubrovskii, Vladimir G. 2014. *Nucleation Theory and Growth of Nanostructures*. *Nucleation Theory and Growth of Nanostructures*.

Fahami, Abbas, Reza Ebrahimi-Kahrizsangi, and Bahman Nasiri-Tabrizi. 2011. "Mechanochemical Synthesis of Hydroxyapatite/Titanium Nanocomposite." *Solid State Sciences* 13 (1): 135–41. doi:10.1016/j.solidstatesciences.2010.10.026.

Fan, Yuwei, Zhi Sun, and Janet Moradian-Oldak. 2009a. "Controlled Remineralization of Enamel in the Presence of Amelogenin and Fluoride." *Biomaterials* 30 (4): 478–83. doi:10.1016/j.biomaterials.2008.10.019.

Figueiredo Macedo de Lima, Joyce, Maria do Carmo Aguiar Jordão Mainardi, Regina Maria Puppin-Rontani, Ubirajara Pereira Rodrigues-Filho, Priscila Christiane Suzy Liporoni, Marcelo Luiz Calegaro, Klaus Rischka, and Flávio Henrique Baggio Aguiar. 2020. "Bioinspired Catechol Chemistry for Dentin Remineralization: A New Approach for the Treatment of Dentin Hypersensitivity." *Dental Materials* 36 (4). Elsevier Inc.: 501–11. doi:10.1016/j.dental.2020.01.012.

Fowler, B 0, E C Moreno, and W E Brown. 1966. "INFRA-RED SPECTRA OF HYDROXYAPATITE, OCTACALCIUM PHOSPHATE AND PYROLYSED OCTA-CALCIUM PHOSPHATE." *Arch. Oral Bid.* Vol. 11.

Fowler, Douglas M., and Stanley Fields. 2014. "Deep Mutational Scanning: A New Style of Protein Science." *Nature Methods*. Nature Publishing Group. doi:10.1038/nmeth.3027.

Gao, Sherry Shiqian, Shinan Zhang, May Lei Mei, Edward Chin Man Lo, and Chun Hung Chu. 2016. "Caries Remineralisation and Arresting Effect in Children by Professionally Applied Fluoride Treatment - a Systematic Review." *BMC Oral Health* 16 (1). doi:10.1186/s12903-016-0171-6.

Gebauer, Denis, Paolo Raiteri, Julian D. Gale, and Helmut Cölfen. 2018. "On Classical and Non-Classical Views on Nucleation." *American Journal of Science* 318 (9). doi:10.2475/09.2018.05.

Gezawi, Moataz El, Uta Christine Wölfle, Rasha Haridy, Riham Fliefel, and Dalia Kaisarly. 2019. "Remineralization, Regeneration, and Repair of Natural Tooth Structure: Influences on the Future of Restorative Dentistry Practice." *ACS Biomaterials Science and Engineering*. American Chemical Society. doi:10.1021/acsbiomaterials.9b00591.

Gil-Bona, Ana, and Felicitas B. Bidlack. 2020. "Tooth Enamel and Its Dynamic Protein Matrix." *International Journal of Molecular Sciences*. MDPI AG. doi:10.3390/ijms21124458.

Goldbourt, U, and H.N. Neufeld. 1986. "Goldbourt-Neufeld-1986-Genetic-Aspects-of-Arteriosclerosis." *American Heart Association, Inc,*.

Gungormus, Mustafa, Hanson Fong, Il Won Kim, John Spencer Evans, Candan Tamerler, and Mehmet Sarikaya. 2008. "Regulation of in Vitro Calcium Phosphate Mineralization by Combinatorially Selected Hydroxyapatite-

Binding Peptides.” *Biomacromolecules* 9 (3): 966–73. doi:10.1021/bm701037x.

Gungormus, Mustafa, Ersin E. Oren, Jeremy A. Horst, Hanson Fong, Marketa Hnilova, Martha J. Somerman, Malcolm L. Snead, Ram Samudrala, Candan Tamerler, and Mehmet Sarikaya. 2012a. “Cementomimeticsconstructing a Cementum-like Biomineralized Microlayer via Amelogenin-Derived Peptides.” *International Journal of Oral Science* 4 (2): 69–77. doi:10.1038/ijos.2012.40.

Hänsch, Robert, and Ralf R. Mendel. 2009. “Physiological Functions of Mineral Micronutrients (Cu, Zn, Mn, Fe, Ni, Mo, B, Cl).” *Current Opinion in Plant Biology*. doi:10.1016/j.pbi.2009.05.006.

Haque, Mainul, Massimo Sartelli, and Seraj Zohurul Haque. 2019. “Dental Infection and Resistance-Global Health Consequences.” *Dentistry Journal*. MDPI Multidisciplinary Digital Publishing Institute. doi:10.3390/dj7010022.

HASSAN MMed, Rosline, Azlan Husin, Sarina Sulong, Surini Yusoff, Muhammad Farid JOHAN, Badrul Hisham YAHAYA, CY Ang, Selamah GHAZALI Dip, Cheong Soon Keng, and Rosline Hassan. 2015. “Guidelines for Nucleic Acid Detection and Analysis in Hematological Disorders.”

Ikoma, Toshiyuki, Atsushi Yamazaki, Satoshi Nakamura, and Masaru Akao. 1999. “Preparation and Structure Refinement of Monoclinic Hydroxyapatite.” *Journal of Solid State Chemistry*. Vol. 144. http://www.idealibrary.comon.

Jensen, M. E. 1999. “Diet and Dental Caries.” *Dental Clinics of North America*. doi:10.1177/0022034515590377.

Jeremias, Fabiano, Mine Koruyucu, Erika C. Küchler, Merve Bayram, Elif B. Tuna, Kathleen Deeley, Ricardo A. Pierri, et al. 2013. “Genes Expressed in Dental Enamel Development Are Associated with Molar-Incisor Hypomineralization.” *Archives of Oral Biology* 58 (10). Elsevier Ltd: 1434–42. doi:10.1016/j.archoralbio.2013.05.005.

Kanazawa, Yasuo, and Masaharu Kamitani. 2006. “Rare Earth Minerals and Resources in the World.” In *Journal of Alloys and Compounds*, 408–412:1339–43. doi:10.1016/j.jallcom.2005.04.033.

Kashyap, Shreyas J., Ravi Sankannavar, and G. M. Madhu. 2021. “Fluoride Sources, Toxicity and Fluorosis Management Techniques – A Brief Review.” *Journal of Hazardous Materials Letters* 2. doi:10.1016/j.hazl.2021.100033.

Kim, Dong Wook, In Sun Cho, Jin Young Kim, Hae Lin Jang, Gill Sang Han, Hyun Seung Ryu, Heungsoo Shin, Hyun Suk Jung, Hyungtak Kim, and Kug Sun Hong. 2010. “Simple Large-Scale Synthesis of Hydroxyapatite Nanoparticles: In Situ Observation of Crystallization Process.” *Langmuir* 26 (1): 384–88. doi:10.1021/la902157z.

Kim, J, DD Arola, L Gu, YK Kim, S Mai, Y Liu - Acta biomaterialia, and undefined 2010. 2023. “Functional Biomimetic Analogs Help Remineralize Apatite-Depleted Demineralized Resin-Infiltrated Dentin via a Bottom–up Approach.” *Elsevier*. Accessed April 25. https://www.sciencedirect.com/science/article/pii/S1742706109005935.

Kirkham, Bioengineering J, A Firth, D Vernals, N Boden-, C Robinson, RC Shore, SJ Brookes, and A Aggeli. n.d. “Self-Assembling Peptide Scaffolds Promote Enamel Remineralization.”

Kleinberg, I, and G N Jenkins. n.d. “THE PH OF DENTAL PLAQUES IN THE DIFFERENT AREAS OF THE MOUTH BEFORE AND AFTER MEALS AND THEIR RELATIONSHIP TO THE PH AND RATE OF FLOW OF RESTING SALIVA.” *Arch. Oral Biok*. Vol. 9.

Kwak, S. Y., A. Litman, H. C. Margolis, Y. Yamakoshi, and J. P. Simmer. 2017. “Biomimetic Enamel Regeneration Mediated by Leucine-Rich Amelogenin Peptide.” *Journal of Dental Research* 96 (5). SAGE Publications Inc.: 524–30. doi:10.1177/0022034516688659.

Lang, Niklaus P., Marc A. Schätzle, and Harald Löe. 2009. “Gingivitis as a Risk Factor in Periodontal Disease.” *Journal of Clinical Periodontology* 36 (SUPPL. 10): 3–8. doi:10.1111/j.1600-051X.2009.01415.x.

Leong Lim, Chin, Chris Byrne, and Jason KW Lee. 2008. “Human Thermoregulation and Measurement of Body Temperature in Exercise and Clinical Settings.” Vol. 37.

Listl, S., J. Galloway, P. A. Mossey, and W. Marcenes. 2015. “Global Economic Impact of Dental Diseases.” In *Journal of Dental Research*, 94:1355–61. SAGE Publications Inc. doi:10.1177/0022034515602879.

Lucena-Aguilar, Gema, Ana María Sánchez-López, Cristina Barberán-Aceituno, José Antonio Carrillo-Ávila, José Antonio López-Guerrero, and Rocío Aguilar-Quesada. 2016. “DNA Source Selection for Downstream Applications Based

on DNA Quality Indicators Analysis." In *Biopreservation and Biobanking*, 14:264–70. Mary Ann Liebert Inc. doi:10.1089/bio.2015.0064.

Lyngstadaas, S P, J C Wohlfahrt, S J Brookes, M L Paine, M L Snead, J E Reseland, and Staale Petter Lyngstadaas. n.d. "Enamel Matrix Proteins; Old Molecules for New Applications."

Markovic, Milenko, and Walter E Brownla. 1993. "Octacalcium Phosphate Carboxylates. 2. Characterization and Structural Considerations." *Chem. Mater*. Vol. 5. https://pubs.acs.org/sharingguidelines.

Marshall, Grayson W, Norimichi Inai, I-Chien Wu Magidi, Mehdi Balooch, John H Kinney, Jungi Tagami, and Sally J Marshall. 1997a. "Dentin Demineralization: Effects of Dentin Depth, PH and Different Acids." *Dent Mater*. Vol. 13.

Mochales, Carolina, Rory M. Wilson, Stephanie E.P. Dowker, and Maria Pau Ginebra. 2011. "Dry Mechanosynthesis of Nanocrystalline Calcium Deficient Hydroxyapatite: Structural Characterisation." *Journal of Alloys and Compounds* 509 (27): 7389–94. doi:10.1016/j.jallcom.2011.04.033.

Mohd Pu'ad, N. A.S., R. H. Abdul Haq, H. Mohd Noh, H. Z. Abdullah, M. I. Idris, and T. C. Lee. 2019. "Synthesis Method of Hydroxyapatite: A Review." In *Materials Today: Proceedings*, 29:233–39. Elsevier Ltd. doi:10.1016/j.matpr.2020.05.536.

Moynihan, Paula, and Poul Erik Petersen. 2004. "Diet, Nutrition and the Prevention of Dental Diseases." *Public Health Nutrition* 7 (1a). doi:10.1079/phn2003589.

Nasiri-Tabrizi, B., Pezhman Honarmandi, R. Ebrahimi-Kahrizsangi, and Peyman Honarmandi. 2009. "Synthesis of Nanosize Single-Crystal Hydroxyapatite via Mechanochemical Method." *Materials Letters* 63 (5): 543–46. doi:10.1016/j.matlet.2008.11.030.

Neel, Ensanya Ali Abou, Anas Aljabo, Adam Strange, Salwa Ibrahim, Melanie Coathup, Anne M. Young, Laurent Bozec, and Vivek Mudera. 2016. "Demineralization–Remineralization Dynamics in Teeth and Bone." *International Journal of Nanomedicine*. doi:10.2147/IJN.S107624.

Nguyen, Nga Kim, Matteo Leoni, Devid Maniglio, and Claudio Migliaresi. 2013. "Hydroxyapatite Nanorods: Soft-Template Synthesis, Characterization and Preliminary in Vitro Tests." *Journal of Biomaterials Applications* 28 (1): 49–61. doi:10.1177/0885328212437065.

Niu, Li Na, Wei Zhang, David H. Pashley, Lorenzo Breschi, Jing Mao, Ji Hua Chen, and Franklin R. Tay. 2014. “Biomimetic Remineralization of Dentin.” *Dental Materials* 30 (1): 77–96. doi:10.1016/j.dental.2013.07.013.

Noren, Karen A., and Christopher J. Noren. 2000. “Construction of High-Complexity Combinatorial Phage Display Peptide Libraries.” *Methods* 23 (2). Academic Press Inc.: 169–78. doi:10.1006/meth.2000.1118.

Orava, Jiri, and A. Lindsay Greer. 2017. “Classical-Nucleation-Theory Analysis of Priming in Chalcogenide Phase-Change Memory.” *Acta Materialia* 139. doi:10.1016/j.actamat.2017.08.013.

Oren, Ersin Emre, Candan Tamerler, Deniz Sahin, Marketa Hnilova, Urartu Ozgur Safak Seker, Mehmet Sarikaya, and Ram Samudrala. 2007. “A Novel Knowledge-Based Approach to Design Inorganic-Binding Peptides.” *Bioinformatics* 23 (21). Oxford University Press: 2816–22. doi:10.1093/bioinformatics/btm436.

Paine, Michael L, Shane N White, Wen Luo, Hanson Fong, Mehmet Sarikaya, and Malcolm L Snead. 2001. “Mini-Review Regulated Gene Expression Dictates Enamel Structure and Tooth Function.”

Pande, Jyoti, Magdalena M. Szewczyk, and Ashok K. Grover. 2010. “Phage Display: Concept, Innovations, Applications and Future.” *Biotechnology Advances*. doi:10.1016/j.biotechadv.2010.07.004.

Peitl, Oscar, Edgar Dutra Zanotto, and Larry L Hench. n.d. “Highly Bioactive P 2 O 5 ±Na 2 O±CaO±SiO 2 Glass-Ceramics.” www.elsevier.com/locate/jnoncrysol.

Petersen, Poul Erik, Denis Bourgeois, Hiroshi Ogawa, Saskia Estupinan-Day, and Charlotte Ndiaye. 2005a. “Policy and Practice The Global Burden of Oral Diseases and Risks to Oral Health.” *Bulletin of the World Health Organization*. Vol. 83.

Peutzfeldt, A., S. Mühlebach, A. Lussi, and S. Flury. 2018. “Marginal Gap Formation in Approximal ‘“bulk Fill”’ Resin Composite Restorations after Artificial Ageing.” *Operative Dentistry* 43 (2). Indiana University School of Dentistry: 180–89. doi:10.2341/17-068-L.

Phatai, Piaw, Cybelle Morales Futalan, Songkot Utara, Pongtanawat Khemthong, and Sirilak Kamonwannasit. 2018. “Structural Characterization of Cerium-Doped Hydroxyapatite Nanoparticles Synthesized by an Ultrasonic-Assisted

Sol-Gel Technique." *Results in Physics* 10 (September). Elsevier B.V.: 956–63. doi:10.1016/j.rinp.2018.08.012.

Pitts, Nigel B., Domenick T. Zero, Phil D. Marsh, Kim Ekstrand, Jane A. Weintraub, Francisco Ramos-Gomez, Junji Tagami, Svante Twetman, Georgios Tsakos, and Amid Ismail. 2017. "Dental Caries." *Nature Reviews Disease Primers* 3 (May). Nature Publishing Group. doi:10.1038/nrdp.2017.30.

Pramanik, Sumit, Avinash Kumar Agarwal, K. N. Rai, and Ashish Garg. 2007. "Development of High Strength Hydroxyapatite by Solid-State-Sintering Process." *Ceramics International* 33 (3): 419–26. doi:10.1016/j.ceramint.2005.10.025.

Pye, A. D., D. E.A. Lockhart, M. P. Dawson, C. A. Murray, and A. J. Smith. 2009. "A Review of Dental Implants and Infection." *Journal of Hospital Infection*. doi:10.1016/j.jhin.2009.02.010.

Ramanan, Sutapa Roy, and Ramanan Venkatesh. 2004. "A Study of Hydroxyapatite Fibers Prepared via Sol-Gel Route." *Materials Letters* 58 (26). Elsevier: 3320–23. doi:10.1016/j.matlet.2004.06.030.

Rath, Siddharth S, Jacob L Rodriguez, Jonathan Francis-Landau, Oliver Nakano-Baker, and Mehmet Sarikaya. n.d. "Deep Directed Evolution of Solid Binding Peptides 1 for Quantitative Big-Data Generation 2 3 Deniz T." doi:10.1101/2021.01.26.428348.

Read, H. H. 1970. *Rutley's Elements of Mineralogy*. *Rutley's Elements of Mineralogy*. doi:10.1007/978-94-011-9769-4.

Reddy, GuntakalaVikram, JayapradaReddy Surakanti, Harikumar Vemisetty, Suryasowjanya Doranala, JayasreeReddy Hanumanpally, and Suryakanth Malgikar. 2019. "Comparative Assessment of Effectiveness of Biomin, NovaMin, Herbal, and Potassium Nitrate Desensitizing Agents in the Treatment of Hypersensitive Teeth: A Clinical Study." *Journal of Dr. NTR University of Health Sciences* 8 (1). Medknow: 24. doi:10.4103/jdrntruhs.jdrntruhs_110_18.

Rehm, I, and W Bonfield. 1997. "Characterization of Hydroxyapatite and Carbonated Apatite by Photo Acoustic FTIR Spectroscopy." *JOURNAL OF MATE RIALS SCIENCE: MATERI ALS IN ME DICINE*. Vol. 8.

Ruan, Qichao, Yuzheng Zhang, Xiudong Yang, Steven Nutt, and Janet Moradian-Oldak. 2013. "An Amelogenin-Chitosan Matrix Promotes Assembly of an

Enamel-like Layer with a Dense Interface." *Acta Biomaterialia* 9 (7). Elsevier Ltd: 7289–97. doi:10.1016/j.actbio.2013.04.004.

Sadat-Shojai, Mehdi, Mohammad Taghi Khorasani, Ehsan Dinpanah-Khoshdargi, and Ahmad Jamshidi. 2013. "Synthesis Methods for Nanosized Hydroxyapatite with Diverse Structures." *Acta Biomaterialia*. Elsevier Ltd. doi:10.1016/j.actbio.2013.04.012.

Sahadat Hossain, Md, and Samina Ahmed. 2023. "FTIR Spectrum Analysis to Predict the Crystalline and Amorphous Phases of Hydroxyapatite: A Comparison of Vibrational Motion to Reflection." *RSC Advances* 13 (21). Royal Society of Chemistry: 14625–30. doi:10.1039/d3ra02580b.

Scalera, F., F. Gervaso, K. P. Sanosh, A. Sannino, and A. Licciulli. 2013. "Influence of the Calcination Temperature on Morphological and Mechanical Properties of Highly Porous Hydroxyapatite Scaffolds." *Ceramics International* 39 (5): 4839–46. doi:10.1016/j.ceramint.2012.11.076.

Schmelzer, Jürn W.P. 2010. "On the Determination of the Kinetic Pre-Factor in Classical Nucleation Theory." In *Journal of Non-Crystalline Solids*. Vol. 356. doi:10.1016/j.jnoncrysol.2010.02.026.

Sharma, Vaibhav, Alagiri Srinivasan, Fredrik Nikolajeff, and Saroj Kumar. 2021. "Biomineralization Process in Hard Tissues: The Interaction Complexity within Protein and Inorganic Counterparts." *Acta Biomaterialia*. doi:10.1016/j.actbio.2020.04.049.

Sheiham, Aubrey. 2005. "Editorials Oral Health, General Health and Quality of Life." *Bulletin of the World Health Organization*. Vol. 83. http://www.who.

Shlaferman, Jacob, Alexander Paige, Krista Meserve, Jason A. Miech, and Aren E. Gerdon. 2019. "Selected DNA Aptamers Influence Kinetics and Morphology in Calcium Phosphate Mineralization." *ACS Biomaterials Science and Engineering* 5 (7). American Chemical Society: 3228–36. doi:10.1021/acsbiomaterials.9b00308.

Silva, C. C., M. P.F. Graça, M. A. Valente, and A. S.B. Sombra. 2007. "Crystallite Size Study of Nanocrystalline Hydroxyapatite and Ceramic System with Titanium Oxide Obtained by Dry Ball Milling." *Journal of Materials Science* 42 (11): 3851–55. doi:10.1007/s10853-006-0474-0.

Smith, George P, and Valery A Petrenko. 1997. "Phage Display." https://pubs.acs.org/sharingguidelines.

Sozen, Tumay, Lale Ozisik, and Nursel Calik Basaran. 2017. “An Overview and Management of Osteoporosis.” *European Journal of Rheumatology* 4 (1). AVES YAYINCILIK A.Ş.: 46–56. doi:10.5152/eurjrheum.2016.048.

Suffo-Pino, Miguel, Miguel Ángel Cauqui-López, Celia Pérez-Muñoz, Daniel Goma-Jiménez, Natalia Fernández-Delgado, and Miriam Herrera-Collado. 2023. “Biphasic Bioceramic Obtained from Byproducts of Sugar Beet Processing for Use in Bioactive Coatings and Bone Fillings.” *Journal of Functional Biomaterials* 14 (10). Multidisciplinary Digital Publishing Institute (MDPI). doi:10.3390/jfb14100499.

Szcześ, Aleksandra, Lucyna Hołysz, and Emil Chibowski. 2017. “Synthesis of Hydroxyapatite for Biomedical Applications.” *Advances in Colloid and Interface Science*. Elsevier B.V. doi:10.1016/j.cis.2017.04.007.

Tamerler, Candan, and Mehmet Sarikaya. 2007. “Molecular Biomimetics: Utilizing Nature’s Molecular Ways in Practical Engineering.” *Acta Biomaterialia*. Elsevier BV. doi:10.1016/j.actbio.2006.10.009.

Taş, A. Cüneyt. 2001. “Molten Salt Synthesis of Calcium Hydroxyapatite Whiskers.” *Journal of the American Ceramic Society* 84 (2). American Ceramic Soc: 295–300. doi:10.1111/j.1151-2916.2001.tb00653.x.

Teshima, Katsuya, Sun Hyung Lee, Mitsuo Sakurai, Yoshitaka Kameno, Kunio Yubuta, Takaomi Suzuki, Toetsu Shishido, Morinobu Endo, and Shuji Oishi. 2009. “Well-Formed One-Dimensional Hydroxyapatite Crystals Grown by an Environmentally Friendly Flux Method.” *Crystal Growth and Design* 9 (6): 2937–40. doi:10.1021/cg900159j.

Thunsiri, Kittiya, Siwasit Pitjamit, Peraphan Pothacharoen, Dumnoensun Pruksakorn, Wasawat Nakkiew, and Wassanai Wattanutchariya. 2020. “The 3D-Printed Bilayer’s Bioactive-Biomaterials Scaffold for Full-Thickness Articular Cartilage Defects Treatment.” *Materials* 13 (15). MDPI AG: 1–26. doi:10.3390/ma13153417.

Tjäderhane, Leo, Marcela R Carrilho, Lorenzo Breschi, Franklin R Tay, and David H Pashley. n.d. “Dentin Basic Structure and Composition-an Overview.”

Touger-Decker, Riva, and Cor van Loveren. 2003. “Sugars and Dental Caries.” *The American Journal of Clinical Nutrition*. doi:10.1093/ajcn/78.4.881s.

Ullmann A, Jacob F, and Monod J. 1967. “Characterization by in Vifro Complement&ion of a Peptide Corresponding to an Operator-Proximal Segment of the Fi-Galactosidase Structural Gene of Escherichia Coli.”

Usman, T., Y. Yu, C. Liu, Z. Fan, and Y. Wang. 2014. “Comparison of Methods for High Quantity and Quality Genomic DNA Extraction from Raw Cow Milk.” *Genetics and Molecular Research* 13 (2). Fundacao de Pesquisas Cientificas de Ribeirao Preto: 3319–28. doi:10.4238/2014.April.29.10.

Varoni, Elena M., Tommaso Zuccheri, Andrea Carletta, Barbara Palazzo, Andrea Cochis, Martino Colonna, and Lia Rimondini. 2017. “In Vitro Efficacy of a Novel Potassium Oxalate Hydrogel for Dentin Hypersensitivity.” *European Journal of Oral Sciences* 125 (2). Blackwell Munksgaard: 151–59. doi:10.1111/eos.12334.

Vekilov, Peter G. 2010. “Nucleation.” *Crystal Growth and Design* 10 (12). doi:10.1021/cg1011633.

Vollenweider, Meret, Tobias J. Brunner, Sven Knecht, Robert N. Grass, Matthias Zehnder, Thomas Imfeld, and Wendelin J. Stark. 2007. “Remineralization of Human Dentin Using Ultrafine Bioactive Glass Particles.” *Acta Biomaterialia* 3 (6). Elsevier BV: 936–43. doi:10.1016/j.actbio.2007.04.003.

Weiner’, Stephen, and Ofer Bar-Yosefa. 1990. “States of Preservation of Bones from Prehistoric Sites in the Near East: A Survey.” *Journal of Archaeological Science*. Vol. 17.

Wezenbeek PM, Van, Hulsebos TJ, and Schoenmakers JG. 1980. “Nucleotide Sequence of the Filamentous Bacteriophage M13 DNA Genome- Comparison with Phage Fd.” *Gene*.

Whaley, SR, DS English, EL Hu, and PF Barbara. 2000. “Selection of Peptides with Semiconductor Binding Specificity for Directed Nanocrystal Assembly.” *Nature*.

Wu, Chien Hsun, I. Ju Liu, Ruei Min Lu, and Han Chung Wu. 2016. “Advancement and Applications of Peptide Phage Display Technology in Biomedical Science.” *Journal of Biomedical Science*. BioMed Central Ltd. doi:10.1186/s12929-016-0223-x.

Wu, Duo, Jiaojiao Yang, Jiyao Li, Liang Chen, Bei Tang, Xingyu Chen, Wei Wu, and Jianshu Li. 2013. “Hydroxyapatite-Anchored Dendrimer for in Situ

Remineralization of Human Tooth Enamel." *Biomaterials* 34 (21): 5036–47. doi:10.1016/j.biomaterials.2013.03.053.

Yang, Zheng Yan, Fei Wang, Keke Lu, Yue Heng Li, and Zhi Zhou. 2016. "Arginine-Containing Desensitizing Toothpaste for the Treatment of Dentin Hypersensitivity: A Meta-Analysis." *Clinical, Cosmetic and Investigational Dentistry* 8 (January). Dove Press: 1. doi:10.2147/CCIDE.S95660.

Yoreo, James J. De, Pupa U.P.A. Gilbert, Nico A.J.M. Sommerdijk, R. Lee Penn, Stephen Whitelam, Derk Joester, Hengzhong Zhang, et al. 2015. "Crystallization by Particle Attachment in Synthetic, Biogenic, and Geologic Environments." *Science*. doi:10.1126/science.aaa6760.

Yucesoy, D. T., H. Fong, C. Gresswell, S. Saadat, W. O. Chung, S. Dogan, and M. Sarikaya. 2018. "Early Caries in an In Vivo Model: Structural and Nanomechanical Characterization." *Journal of Dental Research* 97 (13). SAGE Publications Inc.: 1452–59. doi:10.1177/0022034518789898.

Yucesoy, Deniz T., Hanson Fong, John Hamann, Eric Hall, Sami Dogan, and Mehmet Sarikaya. 2022. "Biomimetic Dentin Repair: Amelogenin-Derived Peptide Guides Occlusion and Peritubular Mineralization of Human Teeth." *ACS Biomaterials Science and Engineering*, March. American Chemical Society. doi:10.1021/acsbiomaterials.2c01039.

Yucesoy, Deniz T., Marketa Hnilova, Kyle Boone, Paul M. Arnold, Malcolm L. Snead, and Candan Tamerler. 2015. "Chimeric Peptides as Implant Functionalization Agents for Titanium Alloy Implants with Antimicrobial Properties." *JOM* 67 (4). Minerals, Metals and Materials Society: 754–66. doi:10.1007/s11837-015-1350-7.

Yucesoy, Deniz T., Dimitry Khatayevich, Candan Tamerler, and Mehmet Sarikaya. 2020. "Rationally Designed Chimeric Solid-binding Peptides for Tailoring Solid Interfaces." *MEDICAL DEVICES & SENSORS* 3 (3). Wiley. doi:10.1002/mds3.10065.

Yucesoy, Deniz Tanil, Banu Taktak Karaca, Sibel Cetinel, Huseyin Burak Caliskan, Esref Adali, Nevin Gul-Karaguler, and Candan Tamerler. 2015. "Direct Bioelectrocatalysis at the Interfaces by Genetically Engineered Dehydrogenase." *Bioinspired, Biomimetic and Nanobiomaterials* 4 (1). ICE Publishing: 79–89. doi:10.1680/bbn.14.00022.

Zhan, Jinhua, Yao Hung Tseng, Jerry C.C. Chan, and Chung Yuan Mou. 2005. “Biomimetic Formation of Hydroxyapatite Nanorods by a Single-Crystal-to-Single-Crystal Transformation.” *Advanced Functional Materials* 15 (12): 2005–10. doi:10.1002/adfm.200500274.

Zin, Melvin T., Hong Ma, Mehmet Sarikaya, and Alex K.Y. Jen. 2005. “Assembly of Gold Nanoparticles Using Genetically Engineered Polypeptides.” *Small* 1 (7): 698–702. doi:10.1002/smll.200400164.